© 2023. Published by The Company of Biologists Ltd | Journal of Cell Science (2023) 136, jcs260684. doi:10.1242/jcs.260684

RESEARCH ARTICLE

The force-dependent filamin A–G3BP1 interaction regulates phase-separated stress granule formation

Ziyi Feng, Zhenfeng Mao, Ziwei Yang, Xiaowei Liu and Fumihiko Nakamura*

ABSTRACT

Filamin A (FLNA) is an actin crosslinking protein that mediates mechanotransduction. External and internal mechanical forces, through the actin cytoskeleton, can induce conformational changes of the FLNA molecule to expose cryptic binding sites for its binding partners. Here, we identified Ras GTPase-activating protein SH3 domain-binding protein 1 (G3BP1) as a new FLNA mechanobinding partner. Unlike other FLNA binding partners to the mechanosensing domain repeat 21 (R21), G3BP1 requires an additional neighboring repeat R22 to interact. We demonstrated that their interaction occurs in the cytosol of living cells in an actin polymerization-dependent manner. We also mapped the FLNA-binding site on G3BP1 and found that a F360A point mutation in the RNA recognition motif disrupts the interaction. RNA interfered with the FLNA–G3BP1 interaction, and FLNA did not localize in RNA-rich stress granules (SGs). Disruption of the interaction was sufficient to promote phase-separated SG formation, and arsenite treatment further stimulated the formation of SGs. Taken together, these data identify G3BP1 as a new mechanobinding protein that interacts with the FLNA mechanosensing domain R21 and suggest that SG formation is partially regulated by mechanical force.

KEY WORDS: Filamin A, FLNA, Ras GTPase-activating protein-binding protein 1, G3BP1, Mechanotransduction, Stress granule, Phase separation, Cytoskeleton

INTRODUCTION

Mechanotransduction is the biological process through which cells sense internal and external mechanical forces and convert them into biochemical signals (Broders-Bondon et al., 2018; Chighizola et al., 2019; Nakamura, 2017; Stewart et al., 2020). Mechanotransduction plays a crucial role in tissue repair and regeneration by controlling cell growth, migration, differentiation and tumorigenesis (Chang et al., 2019; Farge, 2011; Lam and Calvo, 2019; Panciera et al., 2020; Tsata and Beis, 2020; Wozniak and Chen, 2009). Previous studies found that filamin A (FLNA) is a molecule that senses and converts mechanical forces into biochemical signals (Ehrlicher et al., 2011; Nakamura et al., 2014; Razinia et al., 2012). FLNA is the first actin cross-linked protein found in non-muscle cells and can interact with a variety of proteins, including intracellular signaling molecules, adhesion molecules and even transcription factors (Nakamura et al., 2011). Complete loss of Flna expression results in embryonic lethality with severe defects in cardiovascular structure and bone in mice (Feng et al., 2006; Hart et al., 2006; Zhou et al., 2007). In humans, *FLNA* mutations can cause mild to severe consequences such as intellectual disabilities, physical malformations, malignant tumors and heart failure (Robertson, 2005).

FLNA consists of two 280 kDa subunits that self-associate to form a long semi-flexible strand. Each FLNA subunit consists of an N-terminal actin-binding domain (ABD) followed by 24 immunoglobulin-like repeats (IgFLNA or R). The most C-terminal repeat, IgFLNA24, mediates dimerization. The C-terminal domains (R16–23) of FLNA have a unique geometry and a compact structure that responds to physiologically relevant mechanical force through conformational changes (Chen et al., 2013; Nakamura et al., 2011; Ruskamo et al., 2012). More specifically, force-induced unfolding of the R20/R21 pair regulates integrin interaction by exposing a cryptic binding site on R21 (Razinia et al., 2012; Rognoni et al., 2012). Recently, we have established a new method to identify binding partners that specifically interact with the mechanosensitive binding site by using stable isotope labeling by amino acids in cell culture (SILAC) proteomics using the R21–23 region as an affinity ligand (Wang and Nakamura, 2019a; Wang and Nakamura, 2019b). This method identified many potential new binding proteins including smoothelin (SMTN) and fimbacin (encoded by *LUZP1*) that were found to be R21-specific mechanobinding partners (Wang and Nakamura, 2019a; Wang and Nakamura, 2019b).

Ras GTPase-activating protein SH3 domain-binding protein 1 (G3BP1) is an RNA-binding protein that is essential for the formation of stress granules (SGs), which are phase-separated cytoplasmic ribonucleoprotein assemblies that protect RNA from stress (Gal et al., 2016; Matsuki et al., 2013; Aulas et al., 2015; Yang et al., 2020). G3BP1 is also involved in various biological functions, such as cell growth, apoptosis and antiviral responses, and its aberrant expression is often detected in various cancers (Alam and Kennedy, 2019; Liu et al., 2022). Recruitment of G3BP1 to SGs in the cytoplasm is induced by various toxic agents such as arsenite (Tourriere et al., 2003). Although phosphorylation of G3BP1 S149 in intrinsically disordered region (IDR) 1 [IDR1, 143–225 amino acids (aa)] strengthens the interaction with IDR3 (411–466 aa) to form a closed conformation, arsenite induces dephosphorylation of S149 to trigger opening of IDR3 to bind RNA (Tourriere et al., 2003; Yang et al., 2020). G3BP1 and its paralog G3BP2 have both overlapping and distinctive functions (Sidibe et al., 2021). Both G3BP1 and G3BP2 are required for arsenite-induced SG formation, but their phase-separation properties are slightly different each other (Guillén-Boixet et al., 2020).

Here, using R21–22 as an affinity ligand, we identified G3BP1, but not G3BP2, as a new mechanobinding partner of FLNA. We found that G3BP1 does not interact with closed FLNA, but opening of the mechanosensitive cryptic binding site R21 enables their interaction, although R22 is also necessary for the interaction. Such

School of Pharmaceutical Science and Technology, Life Science Platform, Tianjin University, 92 Weijin Road, Nankai District, Tianjin, 300072, China.

*Author for correspondence (fnakamura@tju.edu.cn)

F.N., 0000-0002-6872-4246

Handling Editor: Maria Carmo-Fonseca
Received 4 October 2022; Accepted 3 February 2023

Journal of Cell Science (2023) 136, jcs260684. doi:10.1242/jcs.260684

force-dependent interaction was also detected by proximity ligation assay (PLA) in cells. As G3BP1 is also dimerized through the N-terminal NTF2-like (NTF2L) domain, this dimerization could double the valency for FLNA binding. We show that expression of non-FLNA-binding mutant (F360A) G3BP1 in G3BP1-null cells is sufficient to induce SGs and, furthermore, the formation of SGs requires additional stress such as arsenite treatment. We also found that RNA interferes with the FLNA–G3BP1 interaction and FLNA does not localize in G3BP1-rich SGs. Moreover, we demonstrated that phosphorylation and dephosphorylation of G3BP1 S149 do not regulate the FLNA–G3BP1 interaction. Recent research shows that phosphorylation of S149 in IDR1 strengthens the interaction with IDR3, and then phosphorylated G3BP1 is closed. Furthermore, dephosphorylation of G3BP1, which is induced by arsenite treatment, and an increased concentration of RNA triggers opening of IDR3 to bind RNA (Tourriere et al., 2003; Yang et al., 2020).

Taken together, our results suggest that the release of G3BP1 from FLNA to SGs is regulated by both mechanical force and RNA, and further maturation of SGs requires dephosphorylation of S149 induced by stress.

RESULTS

G3BP1 interacts with the exposed cryptic R21 site of FLNA

A cleft between the β-strands C and D of FLNA R21 was previously identified as being the integrin-binding site, blocked with strand A of the adjacent repeat R20 (Lad et al., 2007) (Fig. 1A). As removal of R20 exposes the CD face (the cleft formed by strands C and D; see Fig. 1A) of R21, we used R21–22 as an affinity ligand to identify a new mechanobinding partner for FLNA. As a negative control, we used R1–2 because the CD faces of R1–2 are structurally different from the CD face of R21 (Fig. 1A). Previously, we used R21–23 as an affinity ligand but opted to use R21–22 to exclude a binding protein for R23, which is also a mechanosensing domain. R22 was attached to R21 to make the ligand spatially more accessible for a binding protein on affinity beads.

FLNA R21–22 and R1–2 were expressed as GST–His fusion proteins in *Escherichia coli*, purified by affinity chromatography, cleaved from the GST–His tag, and covalently attached to NHS-Sepharose beads. The ligands behaved as expected; only R21–22 bound to the cytoplasmic domain of integrin-β7 (771–792 aa) and glycoprotein Ibα (556–577 aa) (Calderwood et al., 2001; Nakamura et al., 2009). Using these affinity beads, we pulled several proteins from the lysate of mouse embryonic fibroblast (MEF) cells that specifically bind to R21–22 (Fig. 1B).

We used SILAC followed by mass spectrometry (MS) analysis to identify specific mechanobinding partners as previously described (Wang and Nakamura, 2019a; Wang and Nakamura, 2019b), although we used two isotope-labeled amino acids (lysine and arginine) in this study. The MS result identified 36 proteins that were enriched by over 2-fold when incubating with FLNA R21–22 (Table S1). Among these proteins were known FLNA binding partners such as smoothelin and fimbacin (Fig. 1C). As we detected multiple peptides of G3BP1 with a high heavy to light (H/L) ratio (Fig. 1C) and G3BP1 was also detected in our previous study (Wang and Nakamura, 2019b), here, we focused on G3BP1.

To determine whether FLNA R21–22 interacts with G3BP1 *in vitro*, we expressed green fluorescent protein (GFP)-tagged G3BP1 in human embryonic kidney (HEK) 293 cells and the expressed protein was pulled down with GST–FLNA R21–22 immobilized on glutathione beads. The bound protein was detected by western blotting against GFP. As expected, GFP–G3BP1 co-precipitated with FLNA R21–22 but not with R1–2 (Fig. 2A). We also found

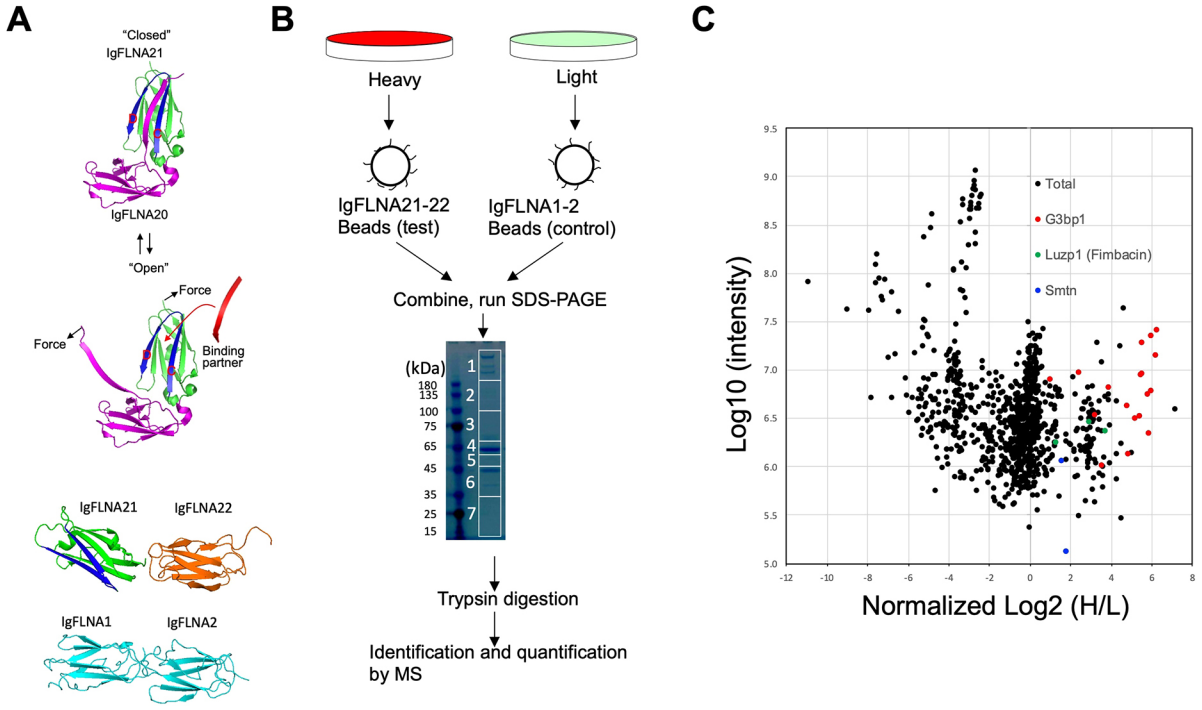

Fig. 1. SILAC-based proteomics of FLNA binding partners. (A) The CD cleft (blue) opens for partner interaction in a force-dependent manner. The FLNA domains used for affinity purification of mechanically regulated FLNA binding partners are shown below. IgFLNA1–2 was used as a negative control. Images were generated from the PDB structures PDB ID:2J3S and PDB ID:2BRQ. Images of IgFLNA1, IgFLNA2 and IgFLNA22 were generated using 3D-JIGSAW (Bates et al., 2001). (B) Schematic representation of the SILAC-based mass spectrometry experiments. (C) Standard scatterplots with normalized $\log_2$(H/L) plotted against $\log_{10}$(intensity) (control versus test) highlighting the distribution of quantified proteins in each MS screening. See also Table S1.

Journal of Cell Science (2023) 136, jcs260684. doi:10.1242/jcs.260684

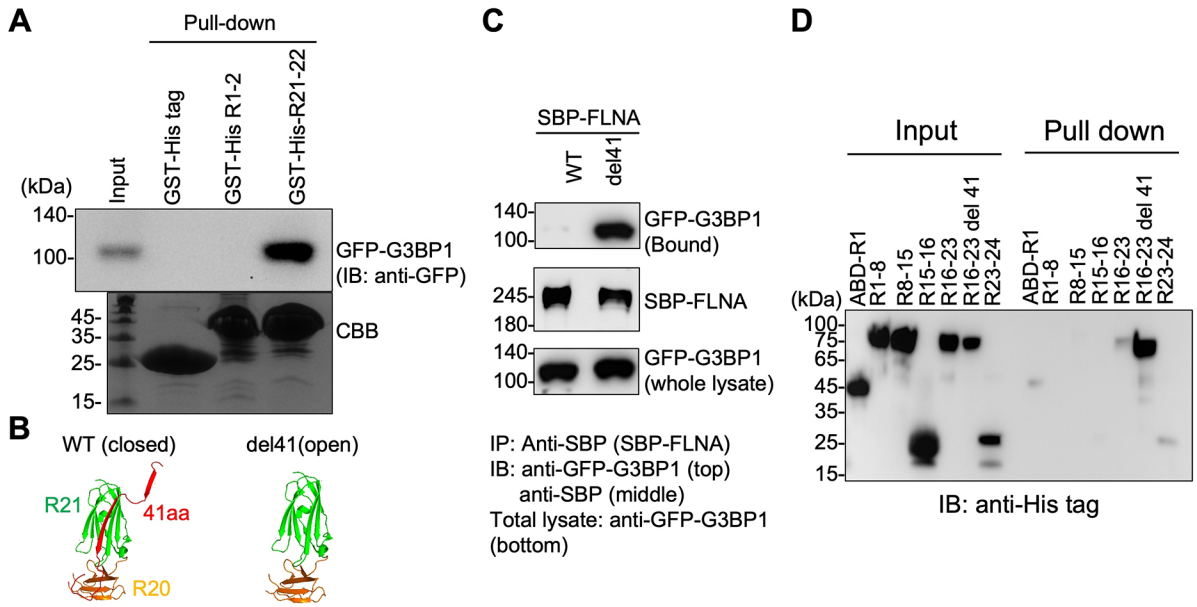

Fig. 2. Selective interaction of G3BP1 with open FLNA. (A) GFP–G3BP1 was expressed in HEK293 cells and the expressed protein was pulled down with GST–His–FLNA fragments. Bound GFP–G3BP1 was detected by western blotting using rabbit anti-GFP antibodies. CBB, Coomassie Brilliant Blue. (B) Wild-type (WT) FLNA R20–21. Deletion of 41 amino acid residues (del41) constitutively exposes the cryptic integrin-binding site. (C) SBP–FLNA was expressed in HEK293 cells. SBP–FLNA was pulled down with streptavidin beads and bound G3BP1 was detected by western blotting using anti-G3BP1 antibodies. (D) Mapping of the G3BP1-binding site on FLNA. Purified His-tagged FLNA fragments were pulled down with GST–G3BP1 immobilized on glutathione beads. ABD-R1 indicates tandem domains of actin-binding domain and repeat 1. Bound His-tagged FLNA fragments were detected by western blotting using an anti-His-tag antibody. IP, immunoprecipitation; IB, immunoblotting.

that mouse G3bp1 can be pulled down with FLNA R21–22 but not with R1–2, consistent with the MS result (see the sequence comparison of human and mouse G3BP1 in Fig. S1).

As lysing the cells would remove mechanical stress on the FLNA molecule, we used a streptavidin-binding protein (SBP)-tagged FLNA del41 construct that constitutively exposes the integrin-β-binding site (deletion of 41 amino acid residues that include strand A of R20 covering the CD face of R21; Fig. 2B) (Pentikainen et al., 2011; van der Flier et al., 2002). GFP–G3BP1, co-expressed with SBP–FLNA in HEK293 cells, was pulled down with SBP–FLNA del41 but not with wild-type (WT) SBP–FLNA (Fig. 2C), suggesting that G3BP1 interacts with the cryptic binding site on R21. To investigate whether G3BP1 interacts with other domains of FLNA, various fragments of FLNA fused to a His tag were incubated with GST–G3BP1 immobilized on glutathione beads. Bound proteins were detected by western blotting against the His tag (Fig. 2D). The result demonstrated that G3BP1 specifically and directly interacts with FLNA R16–23 del41, suggesting that G3BP1 associates with FLNA in a force-dependent manner.

Although multiple proteins bind to FLNA R21 and it is not clear how these proteins compete for the interaction, a high $\log_2$(H/L) ratio in SILAC analysis suggested that the affinity between FLNA and G3BP1 was relatively high compared to that between FLNA and other binding partners (Fig. 1C). In addition, the cellular concentrations of FLNA and G3BP1 were previously estimated as 6 µM and 624 nM, respectively (Wang, 1977; Guillén-Boixet et al., 2020), suggesting that their relative amount is approximately 10:1. However, their relative concentrations are not homogeneous in the cells because FLNA is enriched in actin-rich regions (Nakamura et al., 2011).

FLNA R22 is necessary for G3BP1 interaction

To further narrow down the G3BP1-binding domain of FLNA, each repeat of FLNA fused to the His tag was incubated with GST–G3BP1 immobilized on glutathione beads (Fig. S2A). Unexpectedly, none of the repeats were pulled down with GST–G3BP1. As R21–22 pulled down G3BP1, we wondered whether FLNA R22 is also necessary for the interaction. As speculated, the tandem repeat-containing FLNA R21–22 interacted with G3BP1 but the single repeats R21 and R22 did not (Fig. S2B).

FLNA interacts with the RNA recognition motif of G3BP1 but not with G3BP2

To map the FLNA-binding domain on G3BP1, we divided it into five domains based on its known functional domains (Fig. 3A) (Alam and Kennedy, 2019). Each domain was expressed as a GST fusion protein and immobilized on glutathione beads. The beads were incubated with purified His–eGFP–FLNA R21–22 and bound proteins were detected by western blotting against GFP (Fig. 3B). Interestingly, although domain 4 that contains a RNA recognition motif (RRM) weakly interacted with FLNA R21–22, the addition of domain 5 augmented the interaction (Fig. 3B,C).

FLNA binding partners such as GP1bα, integrins and CFTR use a β-strand that fits into the CD groove formed by FLNA R21 (Kiema et al., 2006; Nakamura et al., 2006; Playford et al., 2010). Alternating residues of the partner β-strand either face towards or away from the groove. Residues facing the groove are indicated by asterisks on the sequence alignment shown in Fig. 4A. Sequence alignment of domain 4 identified a potential FLNA-binding site that is similar to the known FLNA-binding motif (Fig. 4A; Fig. S1). Consistent with this alignment and the previous structural analysis of other binding partners, point mutation of F360 of G3BP1 to alanine was sufficient to disrupt the interaction (Fig. 4B). Moreover, Y363 of G3BP1 was predicted to face away from the groove and not to be involved in the interaction. Consistent with this prediction, Y363F did not disrupt the interaction. G3BP2 also contains a similar sequence but did not interact with FLNA (Fig. 4B). As the

Journal of Cell Science (2023) 136, jcs260684. doi:10.1242/jcs.260684

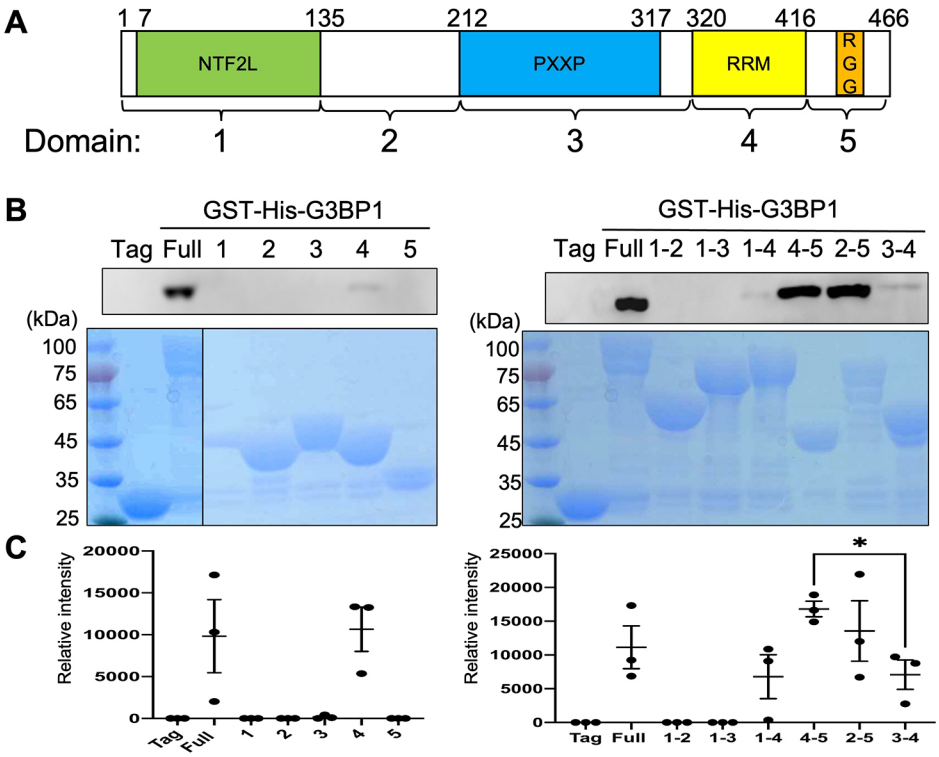

Fig. 3. Schematic structure of G3BP1 and identification of FLNA-binding domains on G3BP1. (A) G3BP1 contains a nuclear transport factor 2-like (NTF2L) domain, proline-rich (PXXP) motif, RNA recognition motif (RRM) and a loosely conserved arginine-glycine-glycine rich box (RGG, also known as intrinsically disordered region 3, IDR3). Domains 1–5 were expressed as GST fusion proteins for binding assays. (B) Purified His–eGFP–FLNA R21–22 was mixed with the indicated GST–G3BP1 domains immobilized on glutathione beads (CBB staining at the bottom). Bound proteins were detected by western blotting against GFP (top). FLNA R21–22 weakly interacts with domain 4 but addition of domain 5 augments the interaction. Note that the bottom panel shows CBB staining of a single gel, with non-relevant lanes removed from the panel on the left. (C) Quantitation of relative band intensity shown in B. Error bars represent s.d. from three independent experiments. *$P \leq 0.05$ (two-tailed, unpaired *t*-test).

differences between G3BP1 and G3BP2 in the potential FLNA-binding motif are two amino acids (M319 and F321 of G3BP2), these residues were mutated to glutamine and tyrosine, respectively. However, mimicking these sites of G3BP2 to those of G3BP1 was not sufficient to induce the binding of G3BP2 to FLNA (Fig. 4C). This is consistent with our finding that domain 4 with a FLNA-binding motif is not sufficient for the stronger interaction between FLNA and G3BP1. As the sequence alignment of domain 5 of the two isoforms shows some difference (Fig. S1), it is likely that this difference defines the specificity. To better understand the

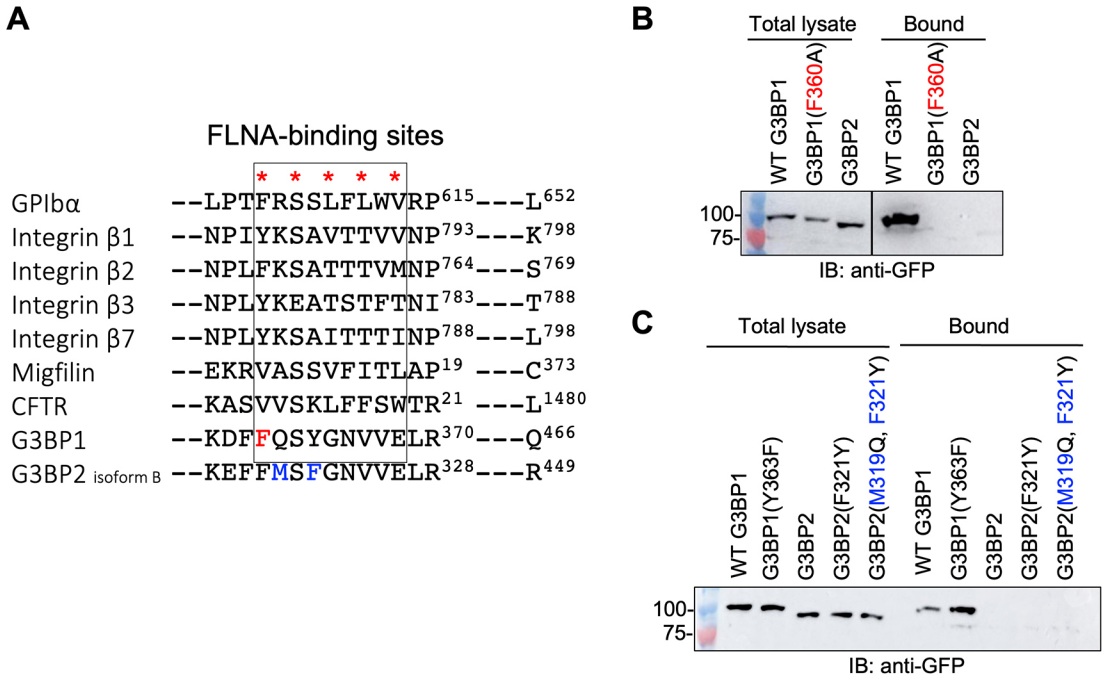

Fig. 4. Identification of critical amino acids of G3BP1 for FLNA interaction. (A) Alignment of the binding interfaces of FLNA binding partners. Amino acids indicated with asterisks are mainly involved in the binding interaction. Point mutation of F360 (red) to alanine (F360A) in G3BP1 is predicted to disrupt the interaction with FLNA. G3BP2 also contains potential FLNA-binding sites. Amino acids in G3BP2 different from G3BP1 are indicated in blue. (B,C) Effect of point mutations of G3BP1 and G3BP2 on FLNA interaction. WT and mutant GFP–G3BP1 and GFP–G3BP2 (isoform B) were expressed in HEK293 cells and cell lysates were mixed with purified GST–FLNA R21–22 immobilized on glutathione beads. Bound proteins were detected by western blotting against GFP. Note that the C-termini of G3BP2 isoforms A and B are identical (isoform B is missing 242–275 aa of G3BP2 isoform A). Note that the mutations M319Q and F321Y of G3BP2 were not sufficient to restore FLNA interaction.

Journal of Cell Science (2023) 136, jcs260684. doi:10.1242/jcs.260684

interaction, structural analysis of FLNA R21–22 and G3BP1 domains 4 and 5 is necessary.

Interaction of G3BP1 with FLNA in living cells

To investigate whether G3BP1 colocalizes with FLNA, we performed indirect immunofluorescence microcopy using mouse monoclonal anti-G3BP1 and rabbit polyclonal anti-FLNA antibodies (Fig. 5A,B; Fig. S3). As G3BP1 is highly expressed in HEK293A, Hela and human skeletal muscle (hsSKM) cells, we investigated the localization of G3BP1 and FLNA in these cells. Although we detected some colocalization (yellow regions in Fig. 5B), G3BP1 was primarily detected in the cytosol, whereas FLNA was mainly localized at cell periphery and extensions. As (1) previous reports showed that G3BP1 localizes in cell adhesions and growing extensions (Arora et al., 2018), (2) some of the extensions were weakly stained with the anti-G3BP1 antibody in our experiment (Fig. 5B) and (3) FLNA is known to localize at cell adhesion (Glogauer et al., 1998), it is possible that G3BP1 interacts with FLNA at these subcellular regions as well.

Because our previous result showed that the opening of R21 occurs not only in the cell edge but also in the cytosol (Nakamura et al., 2014), we investigated whether G3BP1 interacts with FLNA in living cells by performing PLA and fluorescence recovery after photobleaching (FRAP) experiments (Fig. 5C–F). For PLA, we raised FLNA R1-, R22- and R23-specific rabbit polyclonal antibodies and affinity purified and directly labeled the PLA probes. The commercial anti-G3BP1 antibody was also directly labeled with the PLA probe. As FLNA rod-1 (R1–R15) is longer than 50 nm (Nakamura et al., 2007) and the PLA signal is usually detected when the two probes are in close proximity (<40 nm), a combination of R1 and R22 was used as a negative control and a combination of R22 and R23 was used as a positive control. As expected, PLA signals were high when the probes were in close proximity (Fig. 5C,D). The PLA signal was also detected when the two probes were attached to FLNA R22 and G3BP1 antibodies, demonstrating that G3BP1 interacts with FLNA in cells. When cells were treated with latrunculin B to depolymerize actin filaments, the PLA signal was decreased. Arsenite treatment also decreased the PLA signal but did not completely eliminate the signal, presumably because not all G3BP1 is translocated to SGs by arsenite treatment (Fig. S4). The FRAP assay demonstrated that disruption of the interaction by the F360A mutation increases the mobile fraction and shortens the recovery half time ($\tau_{1/2}$). Because the avidity of FLNA dimer to actin filaments is high (Nakamura et al., 2007), the increased mobility of F360A G3BP1 is likely due to disruption of the interaction of G3BP1 with FLNA, indicating that the interaction of G3BP1 with FLNA occurs in the cytosol.

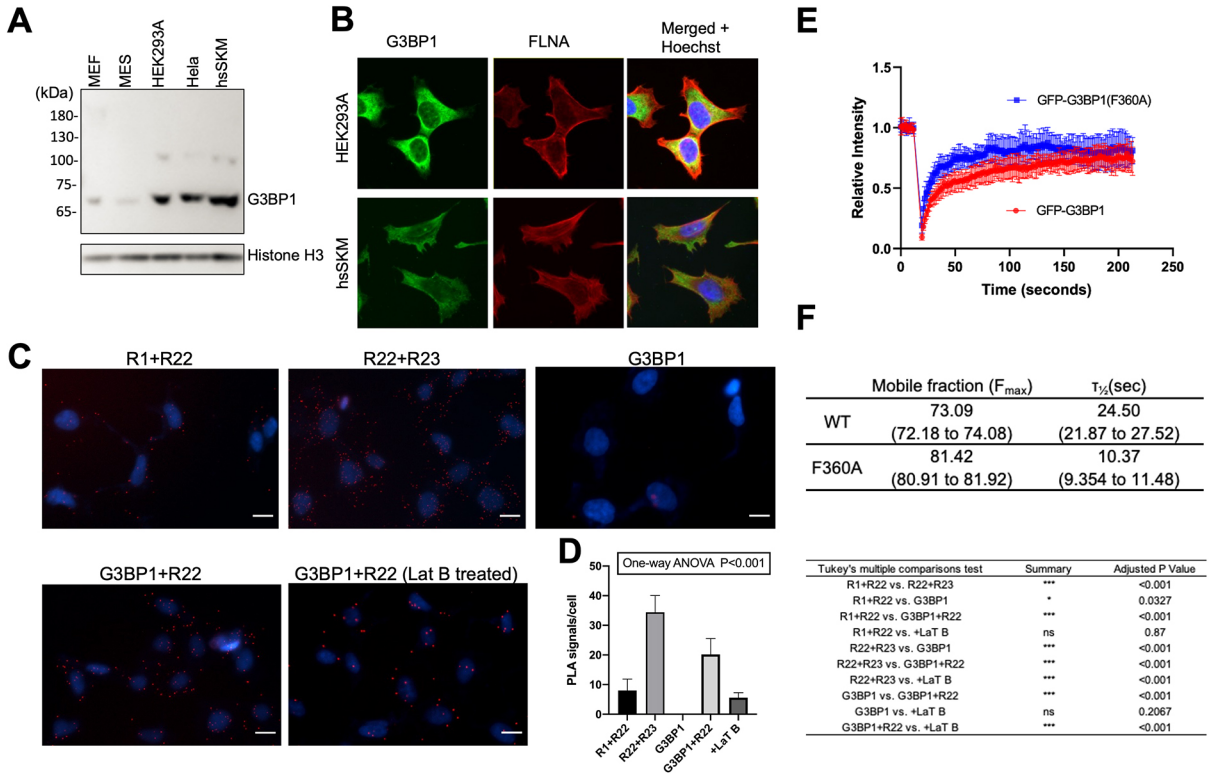

Fig. 5. Interaction of G3BP1 with FLNA in living cells. (A) G3BP1 is expressed in mouse embryonic fibroblasts (MEFs), mouse embryonic stem cells (MES) and HEK293A, Hela and human skeletal muscle (hsSKM) cells. (B) Localization of G3BP1 (green) and FLNA (red) in HEK293A and hsSKM cells. Nuclei in the merged image were stained with Hoechst 33342 (blue). Squares: 100 µm×100 µm. Pearson's correlation coefficients were calculated using the ImageJ plug-in Colocalisation Finder: 0.690±0.104 (HEK293A, *n*=5) and 0.832±0.023 (hsSKM, *n*=5). When one of the two images was rotated by 90°, their Pearson's correlation coefficients changed to 0.113±0.075 (HEK293A, *n*=5) and 0.056±0.170 (hsSKM, *n*=5), respectively. Two-tailed paired *t*-test resulted in $P<0.001$ between before and after 90° rotation for each image. (C) Proximity ligation assay. Representative PLA images in which the PLA signal (red) represents close proximity (<40 nm) between two proteins. The PLA signal is significantly decreased when cells were treated with 5µM latrunculin B (Lat B) for 2 h. Scale bars: 20 µm. (D) The graph (left) shows quantification of PLA signals between FLNA R1 and R22, R22 and R23, G3BP1 alone, G3BP1 and R22, and G3BP1 and R22 with latrunculin B treatment (*n*=5). The table (right) shows summary of statistical analysis. Nuclei were stained by Hoechst 33342 (blue). ns, not significant; $*P\leq0.05$; $***P\leq0.001$. (E) FRAP assay. Curves depict mean values (±s.d.) from measurements of at least seven representative cells. WT (red) and non-FLNA-binding G3BP1 F360A (blue). (F) Summary of FRAP analysis (95% c.i.).

Journal of Cell Science (2023) 136, jcs260684. doi:10.1242/jcs.260684

RNA, not phosphorylation of S149 of G3BP1, regulates the FLNA–G3BP1 interaction

To investigate whether phosphorylation of G3BP1 impacts the binding to FLNA, we expressed phospho-mimicking S149E and non-phosphorylatable S149A mutants (Yang et al., 2020) in HEK293A cells and pulled down G3BP1 with GST–FLNA R21–22 (Fig. 6A). We also tested whether calyculin A, an inhibitor of protein phosphatases 1 and 2A, affects the interaction of endogenous G3BP1 with FLNA R21–22 (Fig. 6B). The results showed that the FLNA–G3BP1 interaction is not phosphorylation dependent. As FLNA interacts with the RNA-binding domains of G3BP1 [both RRM and the arginine-glycine-glycine rich box (RGG, or IDR3)], next, we investigated whether RNA interferes with the FLNA–G3BP1 interaction. We found that RNA disrupted the FLNA–G3BP1 interaction in dose-dependent manner (Fig. 6C).

FLNA does not localize in SGs induced by arsenite

We investigated whether FLNA localizes in SGs in HEK293A and hsSKM cells. Upon arsenite treatment, G3BP1 accumulated in SGs but FLNA did not (Fig. 6D,E), implying that G3BP1 is released from FLNA when it is recruited to SGs. This is consistent with proteomic analyses of SGs that did not detect FLNA (Markmiller et al., 2018). Although arsenite treatment dephosphorylates G3BP1 (Tourriere et al., 2003), dephosphorylation of G3BP1 does not regulates the FLNA–G3BP1 interaction, suggesting that another mechanism is involved in the release of G3BP1 from FLNA.

Expression of F360A G3BP1 is sufficient to induce SGs but further maturation requires an exogenous stress

When WT and F360A G3BP1 were expressed in HEK293A cells using increasing amounts of plasmid DNA, more SGs were formed with mutant G3BP1 with increasing amounts of plasmid DNA (Fig. S5). As HEK293A cells express endogenous G3BP1, which might attenuate the effect of the mutation, we generated G3BP1 knock-out (KO) cells and added back WT and mutant G3BP1 into the KO cells. The levels of expressed G3BP1 proteins were comparable (Fig. S6A). In the endogenous G3BP1-null background, a clearer difference was observed between WT and mutant G3BP1-expressing cells. Moreover, to minimize stress to the

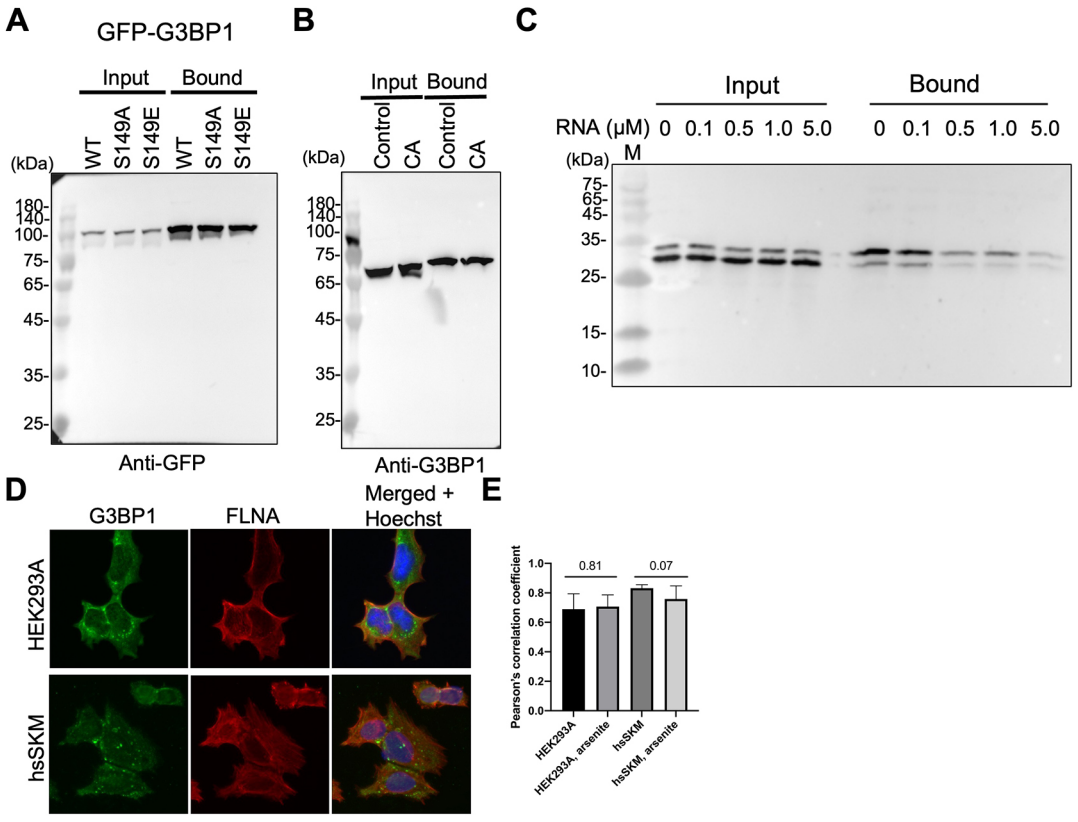

Fig. 6. Interaction of G3BP1 with FLNA is not regulated by phosphorylation but by RNA, and FLNA is not recruited to SGs. (A) HEK293A cells were transfected with AcGFP–G3BP1 (WT, S149A and S149E) and pulled down with GST–FLNA R21–22 immobilized on glutathione beads. Bound proteins were detected by western blotting against GFP. (B) HEK293A cells were treated with 0.1 nM calyculin A (CA) for 30 min and G3BP1 was pulled down with GST–FLNA R21–22 immobilized on glutathione-beads. Bound proteins were detected by western blotting against G3BP1. (C) RNA interferes with the FLNA–G3BP1 interaction in a dose-dependent manner. Purified GST–G3BP1 (1 μM) was immobilized on glutathione beads and incubated with purified His–FLNA R21–22 (1 μM) and increasing amounts of RNA (5′-AGAUUCCACCACAAAGACCC-3′). Bound His–FLNA R21–22 was detected by western blotting using the anti-His-tag antibody. (D) HEK293A and hsSKM cells were treated with 1.5 mM sodium arsenite for 1 h to induce SGs and then stained with anti-G3BP1 (green) and anti-FLNA (red) antibodies. Nuclei in the merged image were stained with Hoechst 33342 (blue). Squares: 100 μm×100 μm. Pearson's correlation coefficients were calculated using the ImageJ plug-in Colocalisation Finder: 0.707±0.079 (HEK293A, *n*=5) and 0.759±0.089 (hsSKM, *n*=5). When one of the two images was rotated by 90°, their Pearson's correlation coefficients changed to 0.170±0.191 (HEK293A, *n*=5) and 0.054±0.084 (hsSKM, *n*=5), respectively. Two-tailed paired *t*-test resulted in $P<0.01$ between before and after 90° rotation for the HEK293A cell and $P<0.001$ for the hsSKM cell. (E) Comparison of Pearson's correlation coefficients of colocalization of FLNA and G3BP1 in HEK and hsSKM cells before and after arsenite treatment. Two-tailed paired *t*-test showed no significant difference between before and after treatment. *P*-values are shown on the top. Error bars represent s.d. from three independent experiments.

Journal of Cell Science (2023) 136, jcs260684. doi:10.1242/jcs.260684

cells, we constructed mammalian expression vectors without Neo^R expression, which is commonly used for selection of transfected cells. We found that with Neo^R expression, more SGs were formed even with lower amounts of plasmid DNA, indicating that Neo^R expression causes some stress (Fig. S6). Therefore, we investigated the effect of F360A mutation on SG formation using plasmids without Neo^R expression in G3BP1 KO cells (Fig. 7). Expression of the mutant G3BP1 induced more SGs than WT, and arsenite treatment promoted SG formation in the cells transfected with WT G3BP1 and in mutant cells transfected with lower amounts of plasmid DNA but not with higher amounts. These results demonstrated that disruption of the G3BP1–FLNA interaction can induce SG formation without additional stress when a sufficient amount of the mutant G3BP1 is expressed. However, additional stress is required when the expression level of G3BP1 is less than the threshold.

Myosin II inhibition induces SG formation

As depolymerization of actin reduces the PLA signal, we tested whether latrunculin B treatment induces SG formation (Fig. S7). Unexpectedly, latrunculin B treatment induced degradation of G3BP1 within 10 min. Although we did not detect any small fragments of G3BP1 by western blotting within the 10–180 kDa range (Fig. S7B), the anti-G3BP1 antibody could still detect the G3BP1 fragment by immunofluorescence microscopy. However, latrunculin B treatment did not induce SG formation (Fig. S7C). Therefore, the effect of latrunculin B on the reduction of PLA signal was not simply by depolymerization of actin. Next, we tested whether myosin II inhibition by blebbistatin induced SGs. Blebbistatin treatment did not induce the degradation of G3BP1 but induced SGs in both HEK293 and MEF cells (Fig. S7C), suggesting that reduction of internal mechanical force releases G3BP1 from FLNA to trigger SG formation.

DISCUSSION

Our data suggest that mechanical force exposes the cryptic G3BP1-binding site of FLNA R21 to interact with the RRM domain of G3BP1 (Fig. 8). G3BP1 contains a conserved FLNA-binding motif in the RRM and point mutation of F360 of G3BP1 to alanine disrupts the interaction, demonstrating that the RRM interacts with FLNA R21 through the FLNA-binding motif. However, the interaction also requires FLNA R22 and RGG (IDR3). As the R22–RGG interaction was not detectable by biochemical assays, we could not conclude how these domains support the FLNA–G3BP1 interaction. Co-crystallography or nuclear magnetic resonance analysis of FLNA R21–22 bound to G3BP1 RRM-RGG would be necessary to answer that question.

Although dephosphorylation (arsenite treatment) converts G3BP1 from a closed to an open conformation, which allows it to bind to RNA to form SGs (Yang et al., 2020), phosphorylation and dephosphorylation do not regulate the FLNA–G3BP1 interaction. We also found that RNA interferes with the FLNA–G3BP1 interaction, which implies that FLNA interferes with the G3BP1–RNA interaction, but FLNA does not localize in G3BP1-rich SGs. These results suggest that release of G3BP1 from FLNA to SGs is regulated by mechanical force and RNA. Conversely, it is also possible that the interaction of G3BP1 with FLNA releases RNA from G3BP1 under mechanical stress. Moreover, we demonstrated that phosphorylation and dephosphorylation of G3BP1 S149 do not regulate the FLNA–G3BP1 interaction. Intriguingly, expression of F360A G3BP1 is sufficient to induce SGs and further formation of SGs requires additional stress such as arsenite treatment. Recent models show that the dephosphorylation of G3BP1 S149 and increased concentration of RNA triggers opening of the IDR3 to bind RNA (Tourriere et al., 2003; Yang et al., 2020). These results suggest that release of G3BP1 from FLNA to SGs is regulated by relaxation of the FLNA molecule and RNA, and further maturation

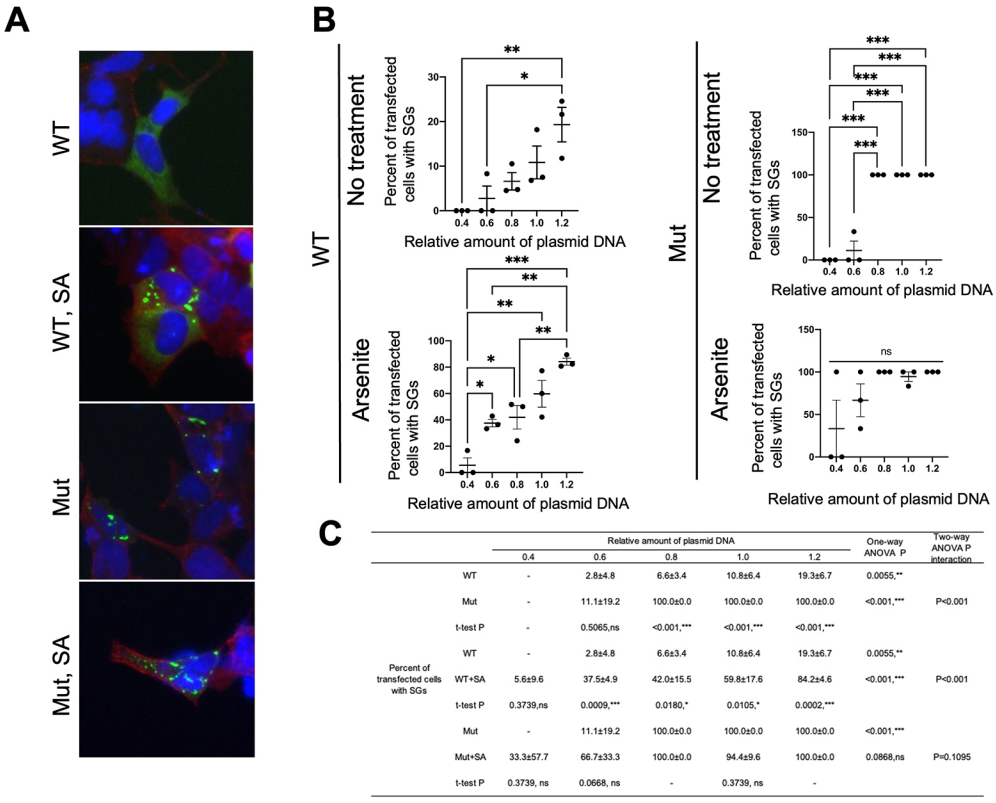

		Relative amount of plasmid DNA 0.4	0.6	0.8	1.0	1.2	One-way ANOVA P	Two-way ANOVA P interaction
Percent of transfected cells with SGs	WT	-	2.8±4.8	6.6±3.4	10.8±6.4	19.3±6.7	0.0055,**	
	Mut	-	11.1±19.2	100.0±0.0	100.0±0.0	100.0±0.0	<0.001,***	P<0.001
	t-test P	-	0.5065,ns	<0.001,***	<0.001,***	<0.001,***		
	WT	-	2.8±4.8	6.6±3.4	10.8±6.4	19.3±6.7	0.0055,**	
	WT+SA	5.6±9.6	37.5±4.9	42.0±15.5	59.8±17.6	84.2±4.6	<0.001,***	P<0.001
	t-test P	0.3739,ns	0.0009,***	0.0180,*	0.0105,*	0.0002,***		
	Mut	-	11.1±19.2	100.0±0.0	100.0±0.0	100.0±0.0	<0.001,***	
	Mut+SA	33.3±57.7	66.7±33.3	100.0±0.0	94.4±9.6	100.0±0.0	0.0868,ns	P=0.1095
	t-test P	0.3739, ns	0.0668, ns	-	0.3739, ns	-		

Fig. 7. Expression of F360A G3BP1 is sufficient to induce SGs but further maturation requires an exogenous stress. (A) Merged images of G3BP1 KO HEK293A cells expressing WT or F360A G3BP1–HA. The HA-tag, FLNA and nucleus were stained in green, red and blue, respectively. Squares: 100×100 µm. Mut, F360A mutation; SA, sodium arsenite. (B) Quantitation of the percentages of cells with SGs from cells expressing G3BP1 by transfection with different relative amounts of plasmid DNA (0.4, 0.6, 0.8, 1.0 and 1.2 times). (C) Statistical analyses. Ten cells were counted for 0.4 (relative amount of plasmid DNA) and over 50 cells were counted for 0.6–1.2 (relative amount of plasmid DNA), from three independent replicates. The results represent the mean±s.d. ns, not significant, P>0.95; *P≤0.05; **P<0.01; ***P≤0.001.

Journal of Cell Science (2023) 136, jcs260684. doi:10.1242/jcs.260684

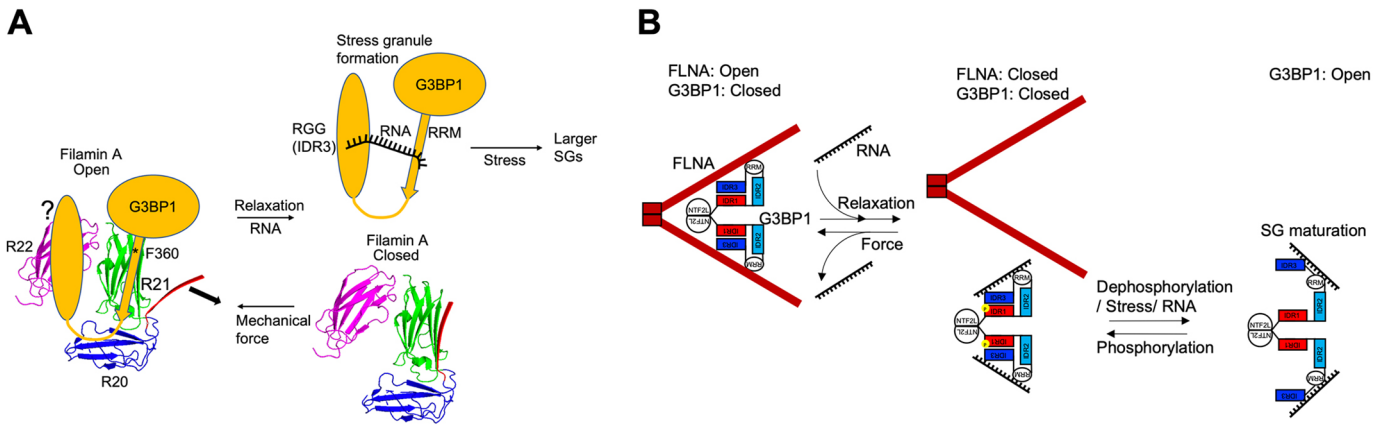

Fig. 8. A model for how mechanical force regulates SG formation. (A) Mechanical force exposes the cryptic G3BP1-binding site of filamin A (FLNA) R21 to interact with the RNA recognition motif (RRM, 320–426 aa) of G3BP1. Point mutation of F360 of G3BP1 to alanine disrupts the interaction. The interaction also requires FLNA R22, which presumably associates with the C-terminal domain of G3BP1 (arginine-glycine rich box, RGG; also known as IDR3). (B) Mechanical stress on FLNA exposes the G3BP1-binding site. Relaxation of the FLNA molecule and/or RNA releases G3BP1 from FLNA to initiate SG formation. Further stress leads to maturation of SGs. Conversely, mechanical forces expose the G3BP1-binding site of FLNA and release RNA from G3BP1.

of SGs requires dephosphorylation of S149 induced by stress (Fig. 8). Conversely, mechanical forces expose the G3BP1-binding site of FLNA, which competes with RNA to release RNA from G3BP1.

Our results also implicated functional differences between G3BP1 and G3BP2. G3BP2 is more efficient in forming SGs (Guillén-Boixet et al., 2020), presumably because it does not compete with FLNA for RNA binding. It is also worth mentioning the implication of the FLNA–G3BP1 interaction in cancer. Expression of G3BP1 is elevated in many cancer cells and knockdown of G3BP1 diminished their proliferation and metastasis (Alam and Kennedy, 2019; Liu et al., 2022). As FLNA R21 also binds to other binding partners such as integrin-β, migfilin, smoothelin and fimbacin, and they are involved in cancer metastasis and growth, it is likely that overexpression of G3BP1 interferes with their interaction with FLNA, thereby promoting tumorigenesis.

MATERIALS AND METHODS

Antibodies and reagents

The antibodies used in this study are summarized in Table S2. The rabbit polyclonal anti-FLNA antibody was previously described (Wang and Nakamura, 2019b). Hoechst 33342 was purchased from Thermo Fisher Scientific. Glutathione-sepharose was purchased from GE Healthcare. Streptavidin (Z02043-5, GenScript) was immobilized on NHS-activated Sepharose 4 Fast Flow beads (GE Healthcare) at 2 mg streptavidin/1 ml beads in accordance with the manufacturer's protocol Calyculin A (A800001) was purchased from Macklin.

Plasmid construction

Human *G3BP1* (UniProt accession ID Q13283) cDNA was amplified by PCR using the primers 5′-CTCAAGCTTGCATGGTGATGGAGAAGCC-TAGTC-3′ and 5′-GCTTCGAATTCTCACTGCCGTGGCGCAAG-3′ with the HEK293 cDNA library as a template, and ligated into the pAcGFP-C1 (Clontech) vector at HindIII/EcoRI sites. Mouse *G3bp1* (UniProt accession ID P97855) cDNA was amplified by PCR using the primers 5′-CTCAAGCTTCGATGGTTATGGAGAAGCCTAGTC-3′ and 5′-CCG-GGATCCTCACTGCCTTGGAGTTGTAATCC-3′ with the MEF cDNA library as a template, and ligated into pAcGFP-C1 at HindIII/BamHI sites. Human G3BP2 cDNA was amplified by PCR using the primers 5′-TCCGAGCTCGAATGGTTATGGAGAAGCCCAG-3′ and 5′-TCC-GAGCTCGAATGGTTATGGAGAAGCCCAG-3′ with HEK293A cDNA library as a template, and ligated into pAcGFP-C1 at SacI/SalI sites. Site-directed mutagenesis was performed using the Q5 site-directed mutagenesis kit (New England Biolabs). For bacterial expression, fragments of *G3BP1* were amplified by PCR and ligated into the pGEX4T-1 (GE Healthcare) or pGEX4T1-HT (Nakamura et al., 2009) vectors. The pSBP (GHVVE-GLAGELEQLRARLEHHPQGQ)-C1 vector was constructed by ligating annealed double-stranded DNA of 5′-CCGGTATGGGCCACGTGGTGG-AGGGCCTGGCCGGCGAGCTGGAGCAGCTGAGAGCCAGACTGG-AGCACCACCCCCAGGGCCAGAGAGAGG-3′ and 5′-GATCCCTCTC-TCTGGCCCTGGGGGTGGTGCTCCAGTCTGGCTCTCAGCTGCTCC-AGCTCGCCGGCCAGGCCCTCCACCACGTGGCCCATA-3′ into the pEGFP-C1 vector (Clontech) digested with AgeI/BamHI. The pSBP-FLNA (WT and del41) vector was constructed in two steps. First, the BamHI/SalI-digested fragment from the PCR product amplified from the actin-binding domain of FLNA was ligated into pSBP-C1 digested with BamHI/SalI. Second, the SalI/NotI-digested fragment from pFLAG-FLNA (WT and del41; Nakamura et al., 2007) was ligated into the pSBP-FLNA N-terminal fragment. pET23-HTb-EGFP-R21–22 and -R1–2 were constructed using the pET23-HTb-EGFP bacterial expression vector (Wang and Nakamura, 2019a) by PCR. To express G3BP1 with a HA tag at the C-terminal, WT and F360A G3BP1 cDNA were ligated into pcDNA3.6-HA (Nakamura et al., 2009). As we found that expression of the Neo gene influenced formation of SGs, the promotor region for the Neo gene was removed.

Protein expression and purification

Bacterial expression was performed with *E. coli* BL21(DE3) Star or C41 (New England Biolabs) cells grown in LB medium in accordance with the manufacturer's protocol. GST- and His-tagged fusion proteins were purified using glutathione-Sepharose and Ni-NTA beads, respectively, in accordance with manufacturer's protocol (GE Healthcare). His–FLNA fragments were expressed and purified as previously described (Playford et al., 2010).

Affinity ligand

Using pFASTBAC-FLNA vector (Nakamura et al., 2002) as the template, FLNA R21–22 (test) and 1–2 (negative control) were cloned into the pGEX4T-HT vector by PCR. The vectors were transformed into *E. coli* C41 cells and protein expression was induced by 0.4 mM isopropyl β-D-thiogalactopyranoside for 2 h. The proteins were affinity purified using glutathione beads and the GST–His tag was cleaved off by TEV protease. Purified FLNA R21–22 and 1–2 were covalently coupled to NHS-activated Sepharose 4 Fast Flow beads (GE Healthcare) at 10 mg per 1 ml of the beads in PBS for 2 h at room temperature. The nonreacted groups of the beads were blocked with 0.1 M Tris-HCl pH 8.0 for 2 h at room temperature, equilibrated with TTBS (50 mM Tris-HCl, pH 7.4, 150 mM NaCl, 1% Triton X-100, 1 mM EGTA and 1 mM β-mercaptoethanol) and stored at 4°C.

Journal of Cell Science (2023) 136, jcs260684. doi:10.1242/jcs.260684

Cell culture, transfection and SILAC labeling

Hela cells, hsSKM cells, mouse embryonic stem cells (MES) and MEF cells were purchased from American Type Collection Center. HEK293A cells were purchased from Thermo Fisher Scientific. These cells were grown in Dulbecco's modified Eagle medium (DMEM; Biological Industries, Israel) supplemented with 10% fetal bovine serum (FBS; Biological Industries) and 1% penicillin-streptomycin. Cells were maintained at 37°C and 5% CO_2. Cells were transfected with polyethylenimine (PEI; 408727, Sigma-Aldrich) (Tom et al., 2008) or LipoGene2000 Star Transfection Reagent (US Everbright). MEF cells were grown for at least six generations in DMEM for SILAC (Thermo Fisher Scientific) supplemented with L-lysine and L-arginine (light) or L-lysine-$^{13}C_6$ and L-arginine-$^{13}C_6$, $^{15}N_4$ (heavy) (Thermo Fisher Scientific) as previously described (Wang and Nakamura, 2019b). Approximately 50 mg of each amino acid was added into every 500 ml of DMEM for SILAC.

Affinity purification for mass spectrometry

Labeled MEF cells were grown on 100 mm tissue culture dishes at about 90% confluency and lysed in 1.5 ml of ice-cold TTBS solution supplemented with complete EDTA-free protease inhibitor cocktail (P8340, Biological Industries) and 2 µM latrunculin B (428020, Thermo Fisher Scientific). Debris was pelleted at 16,000 ***g*** at 4°C for 20 min, and the supernatant was incubated with 20 µl of the affinity beads for 2 h at 4°C. The beads were washed three times with 800 µl of TTBS solution, the bound protein was eluted with LDS sample buffer (NP0007, Thermo Fisher Scientific) containing 50 mM dithiothreitol (DTT) and eluates from both samples (heavy and light) were pooled. The samples were resolved on precast PAGE gels (Novex 4–20% Tris-Gly gel; Thermo Fisher Scientific), stained with colloidal Coomassie Blue (SimplyBlue SafeStain; Thermo Fisher Scientific) and analyzed by liquid chromatography (LC)-MS/MS-based quantification. For this, the lane was cut into seven slices (Fig. 1B), all of which were subsequently subjected to in-gel tryptic digestion.

Mass spectrometry and data analysis

Mass spectrometry, data analysis and database searches were performed as previously described (Cox et al., 2009). Briefly, digested peptides were analyzed by LC-MS/MS on a LTQ-OrbitrapXL hybrid mass spectrometer (Thermo Fisher Scientific). Protein identification and relative quantification was performed using Andromeda and MaxQuant (v1.3.0.5) (Cox et al., 2011). The subsequent bioinformatics and statistical analyses were performed with Perseus 1.4.1.3 (https://maxquant.net/).

Co-precipitation of GFP–G3BP1 with GST–FLNA domains and SBP–FLNA

HEK293A cells were transfected with pAcGFP-G3BP1 with or without pSBP-FLNA (WT and del41) for 36 h and solubilized in TTBS supplemented with complete EDTA-free protease inhibitor cocktail on ice. The lysates were incubated with 30 µl of glutathione beads coated with GST–FLNA fragments (R1–2 and R21–22) or streptavidin-coated beads, respectively, and incubated for 2 h at 4°C. The beads were sedimented and washed with ice-cold TBS-Tx (50 mM Tris-HCl, pH 7.4, 150 mM NaCl, 1 mM EGTA, 1 mM β-mercaptoethanol, 0.1% Triton X-100). Bound proteins were solubilized in SDS sample buffer and separated by a 9% Tris-glycine gel. Immunoblotting was performed using anti-GFP antibody and streptavidin-HRP (ab7403, Abcam).

In vitro binding assay

GST–G3BP1 protein constructs were immobilized on glutathione beads (30 µl) in TBS-Tx and incubated with purified His–eGFP–FLNA R21–22 or R1–2, or His–R21–22 for 1 h at room temperature. To test the effect of RNA on the interaction, increased amounts of RNA (Yang et al., 2020) (5′-AGAUUCCACCACAAAGACCC-3′, Sangon Biotech, China) were added in the mixture. The beads were sedimented and washed with TBS-Tx buffer three times. Bound proteins were solubilized in SDS sample buffer and separated by a 9% or 15% Tris-glycine gel. Immunoblotting was performed using an anti-GFP antibody or anti-His-tag antibody. To identify the G3BP1-binding site on FLNA, purified His-tagged FLNA fragments were incubated with GST–G3BP1 immobilized on glutathione beads. Bound FLNA fragments were detected by western blotting using anti-His mAb conjugated with HRP (1:2000; A7058, Sigma-Aldrich).

Western blotting

Cell lysates in Novex NuPAGE LDS sample buffer with DTT reducing agent (Thermo Fisher Scientific) or SDS sample buffer were loaded onto Novex NuPAGE 4–12% gradient Bis-Tris gels or SDS-PAGE gel. Separated proteins were transferred to nitrocellulose membranes and blocked with blocking buffer [5% non-fat milk powder in TBST (20 mM Tris-HCl, pH 7.4, 150 mM NaCl, 0.05% Tween 20]. Primary antibodies were prepared in this blocking solution and membranes were incubated overnight at 4°C. The membrane was washed in TBST and incubated with HRP-conjugated secondary antibodies in blocking buffer for 1 h at room temperature. The membrane was washed and developed with the HRP substrate (WesternBright ECL, Advansta).

Immunofluorescence microscopy

Cells were plated on a poly-lysine-, gelatin- or fibronectin-coated cover glass, transfected with a plasmid, fixed with 4% formaldehyde in PBS-D (PBS containing 1 mM of Ca^{2+} and Mg^{2+}) for 20 min, rinsed in PBS-D, permeabilized with 0.5% Triton X-100 in TBS for 10 min, rinsed in TBS-Tx, blocked in 2% bovine serum albumin (BSA) in TBS-Tx, and incubated with primary antibodies (anti-G3BP1 and anti-FLNA) for 2 h. After several washes with TBS-Tx, the cells were incubated with secondary antibodies (Thermo Fisher Scientific, Alexa Fluor Plus 488- and Alexa Fluor Plus 594-conjugated IgGs), washed with TBS-Tx, and mounted with mounting media (Spring Bioscience). Cells were imaged on an EVOS FL Auto Imaging System (Thermo Fisher Scientific) fitted with an EVOS Obj, Inf Plan Fluor 20× LWD objective and Plan Fluor 40× LWD, 0.65NA/2.8WD, or on a Leica SP8 with HC PL APO CS2 40×/1.30 oil objective. Images were processed using Image J software [National Institutes of Health (NIH)].

FRAP assay

HEK293A cells expressing WT or mutant AcGFP–G3BP1 were captured onto glass-bottomed dishes coated with fibronectin (03-090-1-01, Biological Industries). Cells were imaged in growth medium without Phenol Red, and with 50 mM HEPES and 1.5% FBS, using a Leica SP8 X confocal microscope. FRAP was performed as described previously (Wang and Nakamura, 2019b). Briefly, the regions of interest (3.19×3.19 µm) were photobleached for 5.0 s at maximum 488-nm laser power. Subsequently, time-lapse images were collected at 5% laser power until the bleached signal reached a stable level. FRAP curves from four independent trials with five cells per trial were derived by fitting the normalized fluorescence at each time point versus time into a one-phase association model plugged into the Prism software. F_{max}, which represents the mobile fraction of the molecule in the bleached region, and $\tau_{1/2}$, which is the time to recover half of the maximum fluorescence and is inversely correlated to the diffusion coefficient, were derived from this curve.

FLNA domain-specific antibodies

DNA constructs encoding human FLNA R1, R22 and R23 were cloned into the pET23-HTa plasmid (Nakamura et al., 2007) and expressed in *E. coli* C41 cells. The cell pellets were lysed by sonication in 20 mM sodium phosphate, 300 mM NaCl, 20 mM imidazole, pH 8.0, and centrifuged at 15,000 ***g*** for 20 min at 4°C. The fusion protein was purified from the supernatant using high affinity Ni-NTA beads (GenScript). After cleavage of the His tag with tobacco etch virus (TEV) protease, the protein was purified by size-exclusion chromatography using an Enrich SEC650 10×300 column (Bio-Rad) in 20 mM sodium phosphate and 150 mM NaCl (pH 7.4). Then, 2 mg of the purified protein was used to immunize a rabbit to generate antiserum (ABclonal). The antibody was affinity purified from the serum using NHS-activated Sepharose (GE Healthcare) beads coated with FLNA R1, R22 or R23 proteins.

Proximity ligation assay

Polyclonal antibodies (against FLNA R1, R22 and R23 and G3BP1) were covalently coupled to oligonucleotides (Table S3). For each conjugation,

50 µg of antibodies in 55 mM phosphate buffer, 150 mM NaCl and 20 mM EDTA (pH 7.2) was activated by addition of a 10-fold molar excess of dibenzyl cyclooctyne NHS ester (DBCO-NHS ester; Jena Bioscience) freshly dissolved in DMSO, and incubated at room temperature for 30 min. The activated antibodies were purified from DBCO-NHS using the 50 K MWCO centrifugal filter (Amicon) and the buffer was exchanged to 55 mM phosphate buffer, 150 mM NaCl and 20 mM EDTA (pH 7.2). The activated antibodies were then mixed with a 2.5-fold molar excess of the respective azide-modified oligonucleotides and incubated overnight at 4°C. Excess oligonucleotides were removed from the reactions using the 50 K MWCO Amicon Ultra-4 centrifuge filter and the buffer was exchanged to PBS containing 5 mM EDTA. The average number of conjugated DBCO molecules per antibody (n^{D-IgG}) was measured and quantified by absorption spectroscopy, using the following equation: $n^{D-IgG}=\frac{c^{D}}{c^{IgG}}$, where the DBCO ($c^{D}$) and antibody ($c^{IgG}$) concentrations were obtained by $c^{D}=\frac{A_{309}}{\varepsilon^{D}_{309}}$ and $c^{IgG}=\frac{A^{c}_{280}}{\varepsilon^{IgG}_{280}}$, respectively. The molar extinction coefficients of the DBCO and IgG antibody are at 309 nm (12,000 M^{-1} cm^{-1}) and 280 nm (204,000 M^{-1} cm^{-1}), respectively. A_{309} is the absorption value of the sample at 309 nm and A^{c}_{280} is the absorption value of the sample corrected by the absorption contribution of DBCO at 280 nm. A^{c}_{280} is calculated by $A^{c}_{280}=A_{280}-(A_{309}\cdot f)$ where the A_{280} is the absorption value of the sample at 280 nm and f the correction factor of DBCO at 280 nm (f=1.1).

HEK293A cells were seeded into a 96-well plate at a density of approximately 20,000 cells/cm^2 in DMEM with 10% FBS supplemented with penicillin and streptomycin and grown for 1–2 days until 70–80% confluency. Cells were fixed with 3.7% formaldehyde for 20 min at room temperature, permeabilized with 0.5% Triton X-100 in PBS for 5 min at room temperature and washed twice with 0.05% Tween-20 in TBS. The cells were blocked by treatment with 250 µg/ml BSA (Genview), 50 µg/ml RNase A (TakaRa), 5 mM EDTA, 11 µg/ml poly(A) (Sigma-Aldrich) and 0.05% Tween-20 in TBS for 2 h at 37°C before overnight incubation at 4°C with 7.5 µg/ml proximity probes, 7.5 µg/ml poly(A), 2.5 mM cysteine, 250 µg/ml BSA and 0.05% Tween-20 in TBS with 5 mM EDTA. Two connector oligonucleotide probes at 125 nM in 10 mM Tris-acetate (pH 7.5), 10 mM magnesium acetate, 50 mM potassium acetate, 0.05 U/ml T4 DNA ligase (New England Biolabs), 250 mM NaCl, 250 µg/ml BSA and 0.05% Tween-20 in H_2O were applied to the cells, and the probes were ligated to form circles using the two oligonucleotides attached to the antibodies as templates. Ligations were performed at 37°C for 1.5 h. The ligated circles were amplified with 0.125 U/ml phi29 DNA polymerase (New England Biolabs) in 50 mM Tris-HCl (pH 7.5), 10 mM $MgCl_2$, 10 mM $(NH_4)_2SO_4$, 250 mM dNTPs, 250 µg/ml BSA and 0.05% Tween-20 at 37°C for 1.5 h. The single-stranded rolling circle amplification (RCA) products were detected by hybridization with 10 nM Cy3-labeled probe in 2× saline sodium citrate, 7.5 µg/ml poly(A), 250 µg/ml BSA and 0.05% Tween-20 for 1 h at 37°C. The nucleus was stained with Hoechst 33342. Cells were manually counted based on positive DAPI staining and PLA spots were identified based on Cy3 fluorescence signal intensity and spot size. PLA interactions per cell were calculated by dividing the PLA spots by the total number of cells in each region of interest. PLA interactions per cell were plotted, and a two-tailed unpaired *t*-test was performed using GraphPad Prism software version 9 (GraphPad Software, La Jolla, CA, USA).

Generation of G3BP1 KO cells

G3BP1 KO HEK293A cells were generated by delivery of Cas9 and target-specific guide RNAs (gRNAs). Oligonucleotides encoding the gRNAs for G3BP1 were designed using CRISPick (https://portals.broadinstitute.org/gpp/public/analysis-tools/sgrna-design) and the selected G3BP1-specific gRNA sequence, 5′-GGAGAAGCCTAGTCCCCTGC-3′, was cloned into BbsI-digested pX330-U6-Chimeric_BB-CBh-hSpCas9 (Addgene plasmid ID: 42230). pX330-G3BP1 plasmids were transfected into HEK293A cells using LipoGene2000 Star transfection reagent according to the manufacturer's protocol. Briefly, HEK293A cells were seeded into a 24-well plate. After 24 h (60–70% confluency), 1 µg pX330-G3BP1 plasmid was added to the well in the presence of LipoGene2000 Star transfection reagent. At 72 h post transfection, cells were cloned on a 96-well plate by serial dilution for another 7 days. Individual clones were expanded, and G3BP1 protein expression was examined by immunoblotting.

Quantitation of SGs

The number of SGs was computationally calculated using NIH ImageJ version 1.53f. G3BP1 KO HEK293A cells were cultured on a 96-well culture plate and then the cells were transfected with different relative amounts of G3BP1 or F360A G3BP1 (0.4, 0.6, 0.8, 1.0 and 1.2 times) by PEI (Tom et al., 2008) or LipoGene 2000 Star transfection Reagent. At 24 h after the transfection, the cells were treated with 1.5 mM sodium arsenite (10048-95-0, Huaxia Reagent) for 60 min. The cells were then fixed and stained for G3BP1. All images were taken with the same settings to allow the comparison of expression level between different conditions. SGs were quantified by outlining each cell using NIH Image J version 1.53f software and setting upper and lower intensity thresholds so that all SGs were included. Cells were scored as SG-positive when they had at least two foci with size ranging from 0.75 to 10 μm^2 in a minimum of three randomly selected cells per condition, and the proportion of cells with SGs (%) was calculated.

Statistics

Data are mean±s.e.m. All experiments were performed at least three times independently. All image analysis was performed by operators who were blinded to the treatments administered. $P>0.05$ was considered as not significant (ns). $^{*}P\leq0.05$, $^{**}P\leq0.01$ and $^{***}P\leq0.001$ was determined by two-tailed paired or unpaired Student's *t*-test, one-way ANOVA, two-way ANOVA or Tukey's multiple comparisons test. Statistical analysis was performed in Graphpad Prism or Excel.

Acknowledgements

We thank the School of Pharmaceutical Science and Technology (SPST) core facility at Tianjin university for their support with MS analysis.

Competing interests

The authors declare no competing or financial interests.

Author contributions

Conceptualization: F.N.; Methodology: Z.F., Z.M., Z.Y., X.L., F.N.; Validation: Z.F., Z.M., Z.Y., X.L., F.N.; Formal analysis: Z.F., Z.M., Z.Y., X.L.; Investigation: Z.F., Z.M., Z.Y., X.L., F.N.; Resources: F.N.; Data curation: Z.F., Z.M., Z.Y., X.L., F.N.; Writing - original draft: Z.F., F.N.; Writing - review & editing: Z.F., F.N.; Visualization: Z.F., Z.M., Z.Y., X.L., F.N.; Supervision: F.N.; Project administration: F.N.; Funding acquisition: F.N.

Funding

This work was supported by grants from the National Natural Science Foundation of China to F.N. (grant number 32070777).

Data availability

The data supporting the findings of this study are available within the article and its supplementary information. All original data and reagents are available from the corresponding author upon reasonable request.

References

Alam, U. and Kennedy, D. (2019). Rasputin a decade on and more promiscuous than ever? A review of G3BPs. *Biochim. Biophys. Acta Mol. Cell Res.* **1866**, 360-370. doi:10.1016/j.bbamcr.2018.09.001

Arora, P. D., He, T., Ng, K. and McCulloch, C. A. (2018). The leucine-rich region of Flightless I interacts with R-ras to regulate cell extension formation. *Mol. Biol. Cell* **29**, 2481-2493. doi:10.1091/mbc.E18-03-0147

Aulas, A., Caron, G., Gkogkas, C. G., Mohamed, N. V., Destroismaisons, L., Sonenberg, N., Leclerc, N., Parker, J. A. and Vande Velde, C. (2015). G3BP1 promotes stress-induced RNA granule interactions to preserve polyadenylated mRNA. *J. Cell Biol.* **209**, 73-84. doi:10.1083/jcb.201408092

Bates, P. A., Kelley, L. A., MacCallum, R. M. and Sternberg, M. J. (2001). Enhancement of protein modeling by human intervention in applying the automatic programs 3D-JIGSAW and 3D-PSSM. *Proteins* **45**, 39-46. doi:10.1002/prot.1168

Broders-Bondon, F., Nguyen Ho-Bouldoires, T. H., Fernandez-Sanchez, M. E. and Farge, E. (2018). Mechanotransduction in tumor progression: the dark side of the force. *J. Cell Biol.* **217**, 1571-1587. doi:10.1083/jcb.201701039

Calderwood, D. A., Huttenlocher, A., Kiosses, W. B., Rose, D. M., Woodside, D. G., Schwartz, M. A. and Ginsberg, M. H. (2001). Increased filamin binding to beta-integrin cytoplasmic domains inhibits cell migration. *Nat. Cell Biol.* **3**, 1060-1068. doi:10.1038/ncb1201-1060

Chang, Y. C., Wu, J. W., Wang, C. W. and Jang, A. C. (2019). Hippo signaling-mediated mechanotransduction in cell movement and cancer metastasis. *Front. Mol. Biosci.* **6**, 157. doi:10.3389/fmolb.2019.00157

Chen, H., Chandrasekar, S., Sheetz, M. P., Stossel, T. P., Nakamura, F. and Yan, J. (2013). Mechanical perturbation of filamin A immunoglobulin repeats 20–21 reveals potential non-equilibrium mechanochemical partner binding function. *Sci. Rep.* **3**, 1642. doi:10.1038/srep01642

Chighizola, M., Dini, T., Lenardi, C., Milani, P., Podesta, A. and Schulte, C. (2019). Mechanotransduction in neuronal cell development and functioning. *Biophys. Rev.* **11**, 701-720. doi:10.1007/s12551-019-00587-2

Cox, J., Matic, I., Hilger, M., Nagaraj, N., Selbach, M., Olsen, J. V. and Mann, M. (2009). A practical guide to the MaxQuant computational platform for SILAC-based quantitative proteomics. *Nat. Protoc.* **4**, 698-705. doi:10.1038/nprot.2009.36

Cox, J., Neuhauser, N., Michalski, A., Scheltema, R. A., Olsen, J. V. and Mann, M. (2011). Andromeda: a peptide search engine integrated into the MaxQuant environment. *J. Proteome Res.* **10**, 1794-1805. doi:10.1021/pr101065j

Ehrlicher, A. J., Nakamura, F., Hartwig, J. H., Weitz, D. A. and Stossel, T. P. (2011). Mechanical strain in actin networks regulates FilGAP and integrin binding to filamin A. *Nature* **478**, 260-263. doi:10.1038/nature10430

Farge, E. (2011). Mechanotransduction in development. *Curr. Top. Dev. Biol.* **95**, 243-265. doi:10.1016/B978-0-12-385065-2.00008-6

Feng, Y., Chen, M. H., Moskowitz, I. P., Mendonza, A. M., Vidali, L., Nakamura, F., Kwiatkowski, D. J. and Walsh, C. A. (2006). Filamin A (FLNA) is required for cell-cell contact in vascular development and cardiac morphogenesis. *Proc. Natl. Acad. Sci. USA* **103**, 19836-19841. doi:10.1073/pnas.0609628104

Gal, J., Kuang, L., Barnett, K. R., Zhu, B. Z., Shissler, S. C., Korotkov, K. V., Hayward, L. J., Kasarskis, E. J. and Zhu, H. (2016). ALS mutant SOD1 interacts with G3BP1 and affects stress granule dynamics. *Acta Neuropathol.* **132**, 563-576. doi:10.1007/s00401-016-1601-x

Glogauer, M., Arora, P., Chou, D., Janmey, P. A., Downey, G. P. and McCulloch, C. A. (1998). The role of actin-binding protein 280 in integrin-dependent mechanoprotection. *J. Biol. Chem.* **273**, 1689-1698. doi:10.1074/jbc.273.3.1689

Guillén-Boixet, J., Kopach, A., Holehouse, A. S., Wittmann, S., Jahnel, M., Schlüßler, R., Kim, K., Trussina, I. R. E. A., Wang, J., Mateju, D. et al. (2020). RNA-induced conformational switching and clustering of G3BP drive stress granule assembly by condensation. *Cell* **181**, 346-361. doi:10.1016/j.cell.2020.03.049

Hart, A. W., Morgan, J. E., Schneider, J., West, K., McKie, L., Bhattacharya, S., Jackson, I. J. and Cross, S. H. (2006). Cardiac malformations and midline skeletal defects in mice lacking filamin A. *Hum. Mol. Genet.* **15**, 2457-2467. doi:10.1093/hmg/ddl168

Kiema, T., Lad, Y., Jiang, P., Oxley, C. L., Baldassarre, M., Wegener, K. L., Campbell, I. D., Ylanne, J. and Calderwood, D. A. (2006). The molecular basis of filamin binding to integrins and competition with talin. *Mol. Cell* **21**, 337-347. doi:10.1016/j.molcel.2006.01.011

Lad, Y., Kiema, T., Jiang, P., Pentikainen, O. T., Coles, C. H., Campbell, I. D., Calderwood, D. A. and Ylanne, J. (2007). Structure of three tandem filamin domains reveals auto-inhibition of ligand binding. *EMBO J.* **26**, 3993-4004. doi:10.1038/sj.emboj.7601827

Lam, M. and Calvo, F. (2019). Regulation of mechanotransduction: emerging roles for septins. *Cytoskeleton (Hoboken)* **76**, 115-122. doi:10.1002/cm.21485

Liu, S., Tian, S., Lin, T., He, X., Eze Ideozu, J., Wang, R., Wang, Y., Yue, D. and Geng, H. (2022). G3BP1 regulates breast cancer cell proliferation and metastasis by modulating PKCzeta. *Front. Genet.* **13**, 1034889. doi:10.3389/fgene.2022.1034889

Markmiller, S., Soltanieh, S., Server, K. L., Mak, R., Jin, W., Fang, M. Y., Luo, E. C., Krach, F., Yang, D., Sen, A. et al. (2018). Context-dependent and disease-specific diversity in protein interactions within stress granules. *Cell* **172**, 590-604.e13. doi:10.1016/j.cell.2017.12.032

Matsuki, H., Takahashi, M., Higuchi, M., Makokha, G. N., Oie, M. and Fujii, M. (2013). Both G3BP1 and G3BP2 contribute to stress granule formation. *Genes Cells* **18**, 135-146. doi:10.1111/gtc.12023

Nakamura, F. (2017). Mechanotransduction in blood cells. *Asia Pac. J. Blood Types Genes* **1**, 1-9. doi:10.46701/APJBG.20170117017

Nakamura, F., Osborn, E., Janmey, P. A. and Stossel, T. P. (2002). Comparison of filamin A-induced cross-linking and Arp2/3 complex-mediated branching on the mechanics of actin filaments. *J. Biol. Chem.* **277**, 9148-9154. doi:10.1074/jbc.M111297200

Nakamura, F., Pudas, R., Heikkinen, O., Permi, P., Kilpelainen, I., Munday, A. D., Hartwig, J. H., Stossel, T. P. and Ylanne, J. (2006). The structure of the GPIb-filamin A complex. *Blood* **107**, 1925-1932. doi:10.1182/blood-2005-10-3964

Nakamura, F., Osborn, T. M., Hartemink, C. A., Hartwig, J. H. and Stossel, T. P. (2007). Structural basis of filamin A functions. *J. Cell Biol.* **179**, 1011-1025. doi:10.1083/jcb.200707073

Nakamura, F., Heikkinen, O., Pentikainen, O. T., Osborn, T. M., Kasza, K. E., Weitz, D. A., Kupiainen, O., Permi, P., Kilpelainen, I., Ylanne, J. et al. (2009). Molecular basis of filamin A-FilGAP interaction and its impairment in congenital disorders associated with filamin A mutations. *PLoS ONE* **4**, e4928. doi:10.1371/journal.pone.0004928

Nakamura, F., Stossel, T. P. and Hartwig, J. H. (2011). The filamins: organizers of cell structure and function. *Cell Adh. Migr.* **5**, 160-169. doi:10.4161/cam.5.2.14401

Nakamura, F., Song, M., Hartwig, J. H. and Stossel, T. P. (2014). Documentation and localization of force-mediated filamin A domain perturbations in moving cells. *Nat. Commun.* **5**, 4656. doi:10.1038/ncomms5656

Panciera, T., Citron, A., Di Biagio, D., Battilana, G., Gandin, A., Giulitti, S., Forcato, M., Bicciato, S., Panzetta, V., Fusco, S. et al. (2020). Reprogramming normal cells into tumour precursors requires ECM stiffness and oncogene-mediated changes of cell mechanical properties. *Nat. Mater.* **19**, 797-806. doi:10.1038/s41563-020-0615-x

Pentikainen, U., Jiang, P., Takala, H., Ruskamo, S., Campbell, I. D. and Ylanne, J. (2011). Assembly of a filamin four-domain fragment and the influence of splicing variant-1 on the structure. *J. Biol. Chem.* **286**, 26921-26930. doi:10.1074/jbc.M110.195958

Playford, M. P., Nurminen, E., Pentikainen, O. T., Milgram, S. L., Hartwig, J. H., Stossel, T. P. and Nakamura, F. (2010). Cystic fibrosis transmembrane conductance regulator interacts with multiple immunoglobulin domains of filamin A. *J. Biol. Chem.* **285**, 17156-17165. doi:10.1074/jbc.M109.080523

Razinia, Z., Makela, T., Ylanne, J. and Calderwood, D. A. (2012). Filamins in mechanosensing and signaling. *Annu. Rev. Biophys.* **41**, 227-246. doi:10.1146/annurev-biophys-050511-102252

Robertson, S. P. (2005). Filamin A: phenotypic diversity. *Curr. Opin. Genet. Dev.* **15**, 301-307. doi:10.1016/j.gde.2005.04.001

Rognoni, L., Stigler, J., Pelz, B., Ylanne, J. and Rief, M. (2012). Dynamic force sensing of filamin revealed in single-molecule experiments. *Proc. Natl. Acad. Sci. USA* **109**, 19679-19684. doi:10.1073/pnas.1211274109

Ruskamo, S., Gilbert, R., Hofmann, G., Jiang, P., Campbell, I. D., Ylanne, J. and Pentikainen, U. (2012). The C-terminal rod 2 fragment of filamin A forms a compact structure that can be extended. *Biochem. J.* **446**, 261-269. doi:10.1042/BJ20120361

Sidibe, H., Dubinski, A. and Vande Velde, C. (2021). The multi-functional RNA-binding protein G3BP1 and its potential implication in neurodegenerative disease. *J. Neurochem.* **157**, 944-962. doi:10.1111/jnc.15280

Stewart, S., Darwood, A., Masouros, S., Higgins, C. and Ramasamy, A. (2020). Mechanotransduction in osteogenesis. *Bone Joint Res.* **9**, 1-14. doi:10.1302/2046-3758.91.BJR-2019-0043.R2

Tom, R., Bisson, L. and Durocher, Y. (2008). Transfection of HEK293-EBNA1 cells in suspension with linear PEI for production of recombinant proteins. *CSH Protoc* **2008**, pdb prot4977.

Tourriere, H., Chebli, K., Zekri, L., Courselaud, B., Blanchard, J. M., Bertrand, E. and Tazi, J. (2003). The RasGAP-associated endoribonuclease G3BP assembles stress granules. *J. Cell Biol.* **160**, 823-831. doi:10.1083/jcb.200212128

Tsata, V. and Beis, D. (2020). In full force. mechanotransduction and morphogenesis during homeostasis and tissue regeneration. *J. Cardiovasc. Dev. Dis.* **7**, 40. doi:10.3390/jcdd7040040

van der Flier, A., Kuikman, I., Kramer, D., Geerts, D., Kreft, M., Takafuta, T., Shapiro, S. S. and Sonnenberg, A. (2002). Different splice variants of filamin-B affect myogenesis, subcellular distribution, and determine binding to integrin [beta] subunits. *J. Cell Biol.* **156**, 361-376. doi:10.1083/jcb.200103037

Wang, K. (1977). Filamin, a new high-molecular-weight protein found in smooth muscle and nonmuscle cells. Purification and properties of chicken gizzard filamin. *Biochemistry.* **16**, 1857-1865. doi:10.1021/bi00628a015

Wang, J. and Nakamura, F. (2019a). Identification of Filamin a mechanobinding partner II: fimbacin is a novel actin cross-linking and filamin a binding protein. *Biochemistry* **58**, 4737-4743. doi:10.1021/acs.biochem.9b00101

Wang, L. and Nakamura, F. (2019b). Identification of filamin a mechanobinding partner I: smoothelin specifically interacts with the filamin a mechanosensitive domain 21. *Biochemistry* **58**, 4726-4736. doi:10.1021/acs.biochem.9b00100

Wozniak, M. A. and Chen, C. S. (2009). Mechanotransduction in development: a growing role for contractility. *Nat. Rev. Mol. Cell Biol.* **10**, 34-43. doi:10.1038/nrm2592

Yang, P., Mathieu, C., Kolaitis, R. M., Zhang, P., Messing, J., Yurtsever, U., Yang, Z., Wu, J., Li, Y., Pan, Q. et al. (2020). G3BP1 is a tunable switch that triggers phase separation to assemble stress granules. *Cell* **181**, 325-345.e28. doi:10.1016/j.cell.2020.03.046

Zhou, X., Boren, J. and Akyurek, L. M. (2007). Filamins in cardiovascular development. *Trends Cardiovasc. Med.* **17**, 222-229. doi:10.1016/j.tcm.2007.08.001

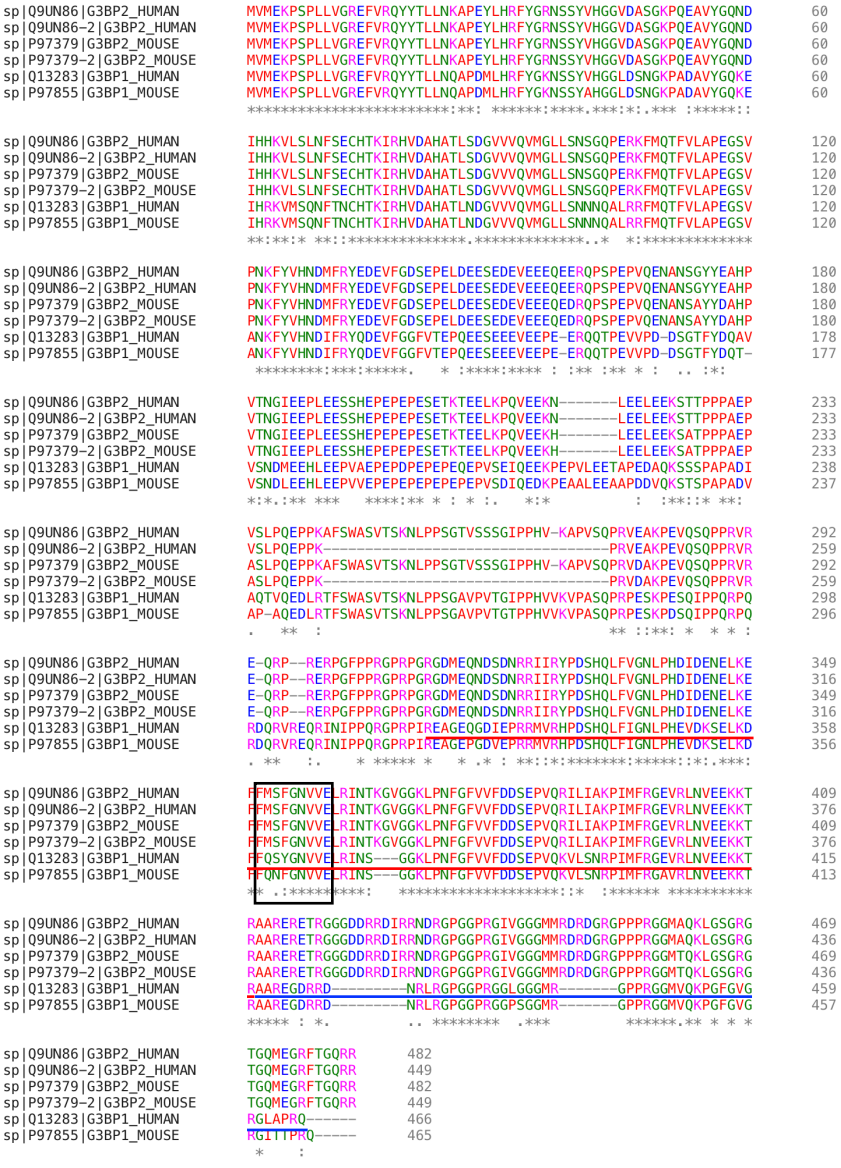

Fig. S1. Amino acid alignment of human and mouse G3BP1 and G3BP2. The alignment was generated by Clustal Omega. FLNA-binding site is indicated in a square. Red underline indicates domain 4 (320-416) and blue underline indicates domain 5 (417-466) in Fig. 4.

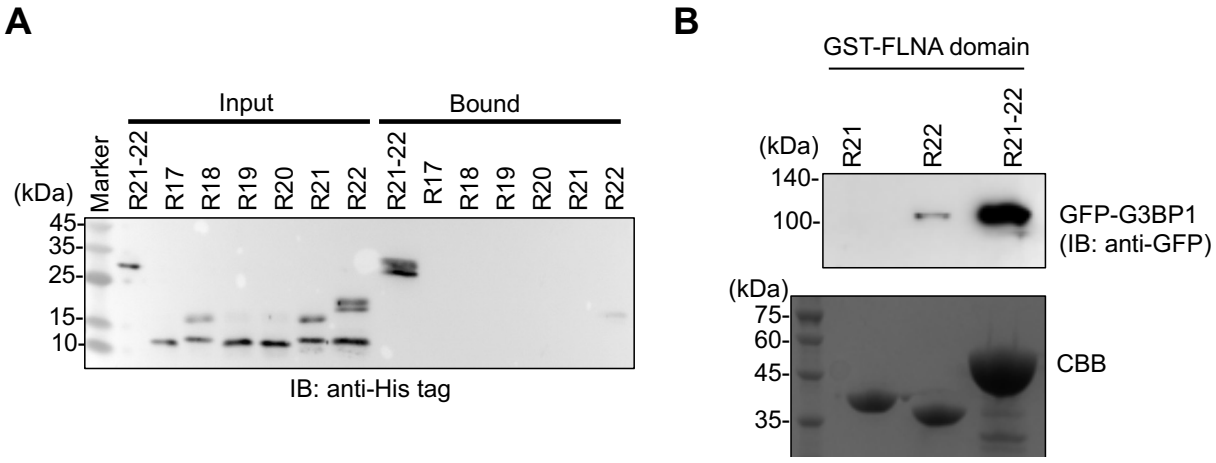

Fig. S2. FLNA R22 is necessary for FLNA-G3BP1 interaction.

(A) Purified His-tag FLNA repeats were incubated with GST-G3BP1 immobilized on glutathione beads. Bound protein was detected by western blotting against His-tag. Note that no bound protein was detected. **(B)** GFP-G3BP1 expressed in HEK 293 cells was pulled down with GST-FLNA R21, R22, and R21-22 immobilized on glutathione beads. Bound protein was detected by western blotting against GFP.

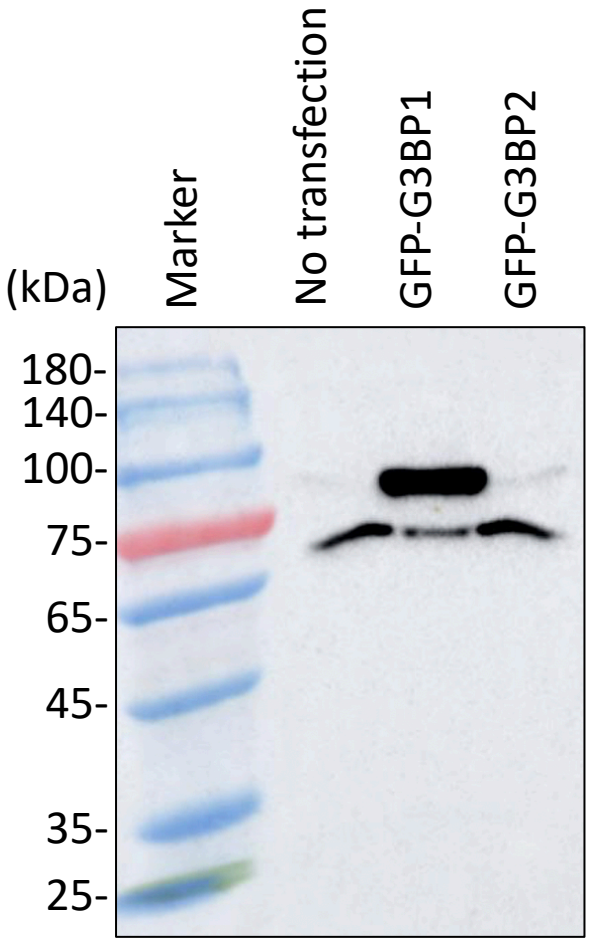

Fig. S3. Mouse monoclonal anti-G3BP1 antibody specifically interacts with G3BP1. GFP-G3BP1 and G3BP2 were expressed in HEK293 cells. The cell lysates were blotted using monoclonal anti-G3BP1 antibody (Proteintech, 66486-1-Ig). Note that anti-G3BP1 antibody recognizes endogenous G3BP1 and GFP-G3BP1 but not GFP-G3BP2.

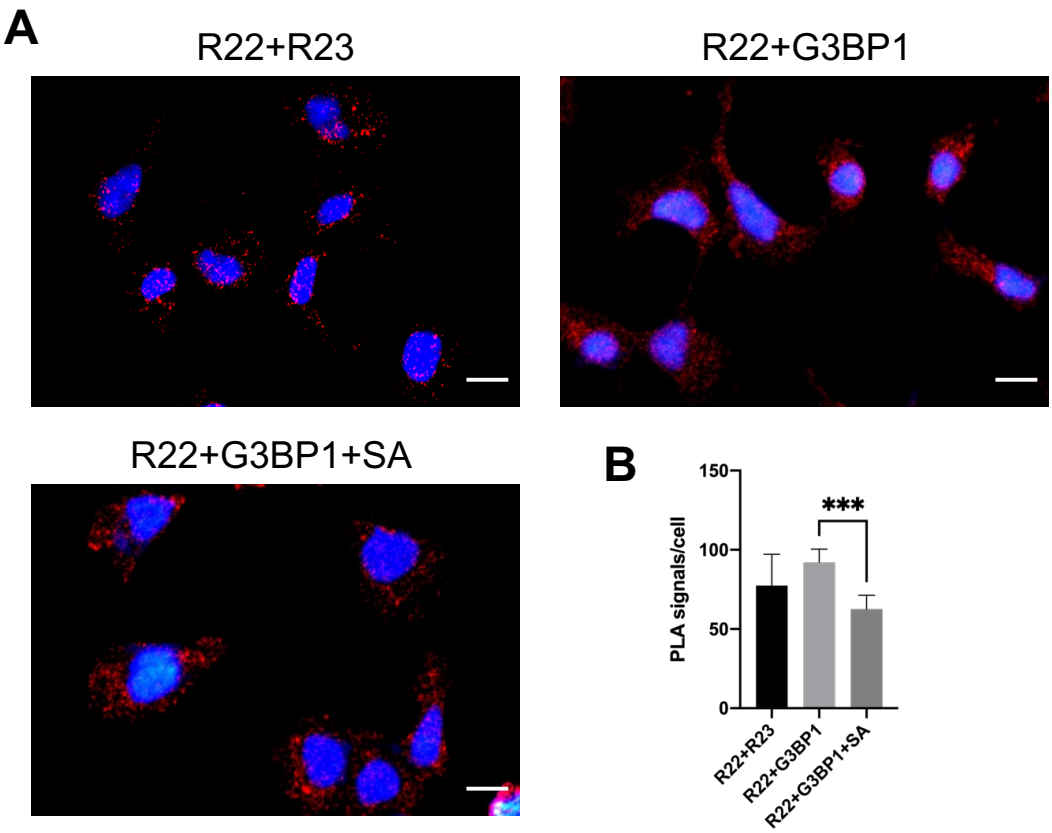

Fig. S4. PLA signal is significantly decreased when cells are treated with sodium arsenite. (**A**) Proximity ligation assay. Representative PLA images where the PLA signal (red) represents close proximity (<40nm) between two proteins. PLA signal is significantly decreased when cells are treated with 1.5 mM sodium arsenite (SA) for 1h. Scale bars: 20µm. (**B**) Graph shows quantification of PLA signals. (***, $P < 0.001$). Error bars represent S.D. from five independent counts.

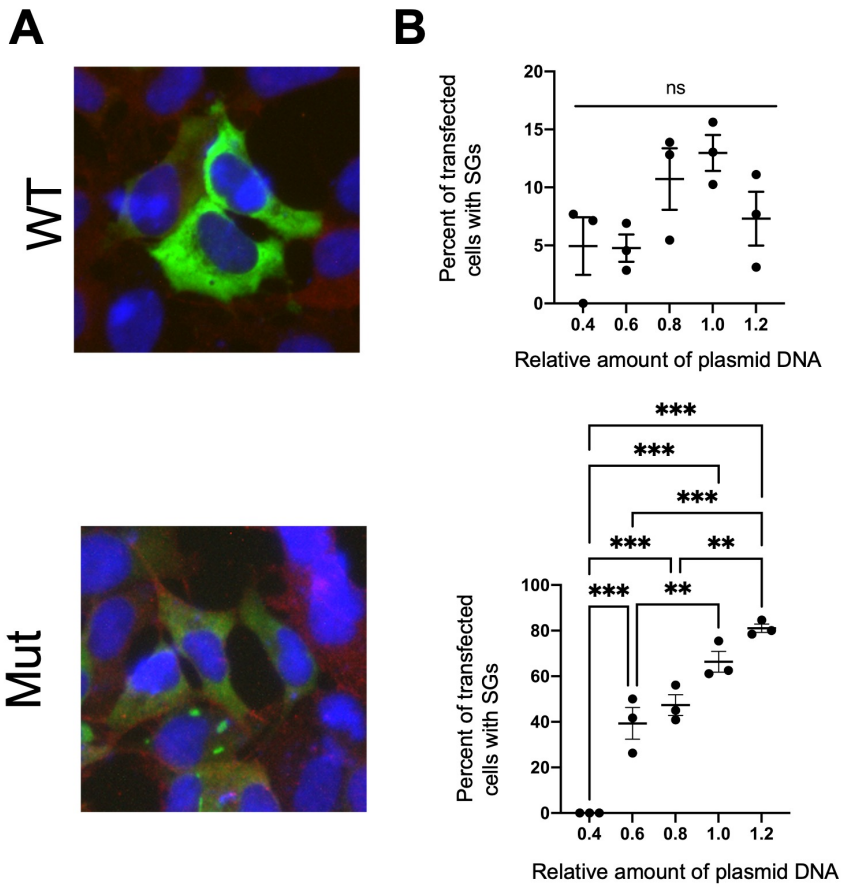

C

		Relative amount of plasmid DNA					One-way ANOVA P	Two-way ANOVA P interaction
		0.4	0.6	0.8	1.0	1.2		
Percent of transfected cells with SGs	WT	4.9±4.3	4.8±2.0	10.7±4.6	13.0±2.7	7.3±4.0	0.0764, ns	
	Mut	-	39.3±12.0	47.3±7.9	66.4±7.9	81.0±3.2	<0.001,***	P<0.001
	t-test P	0.1167, ns	0.0080, **	0.0022, **	0.0004, ***	<0.001, ***		

Fig. S5. Expression of WT and F360A G3BP1 in HEK293A cells.

(**A**) Merged images of HEK293A cells expressing WT or mutant G3BP1-HA. HA-tag, FLNA, and nucleus were stained in green, red, and blue, respectively. 100 × 100 μm. (**B**) Quantitation of cells exogenously expressing G3BP1 by transfection of different relative amount of plasmid DNA (0.4, 0.6, 0.8, 1.0, 1.2 times). P values are presented by * ($P \leqslant 0.05$), ** ($P < 0.01$) or *** ($P \leqslant 0.001$) on the graph, ns (not significant). Error bars represent S.D. from three independent counts. (**C**) Statistical analyses. Ten cells were counted for 0.4 (relative amount of plasmid DNA) and over 50 cells were counted for 0.6~1.2 (relative amount of plasmid DNA), from three independent replicates. The results shown represent the mean (± S.D.) for three independent experiments. t-Test values are given for comparison of results in WT v.s. Mut.

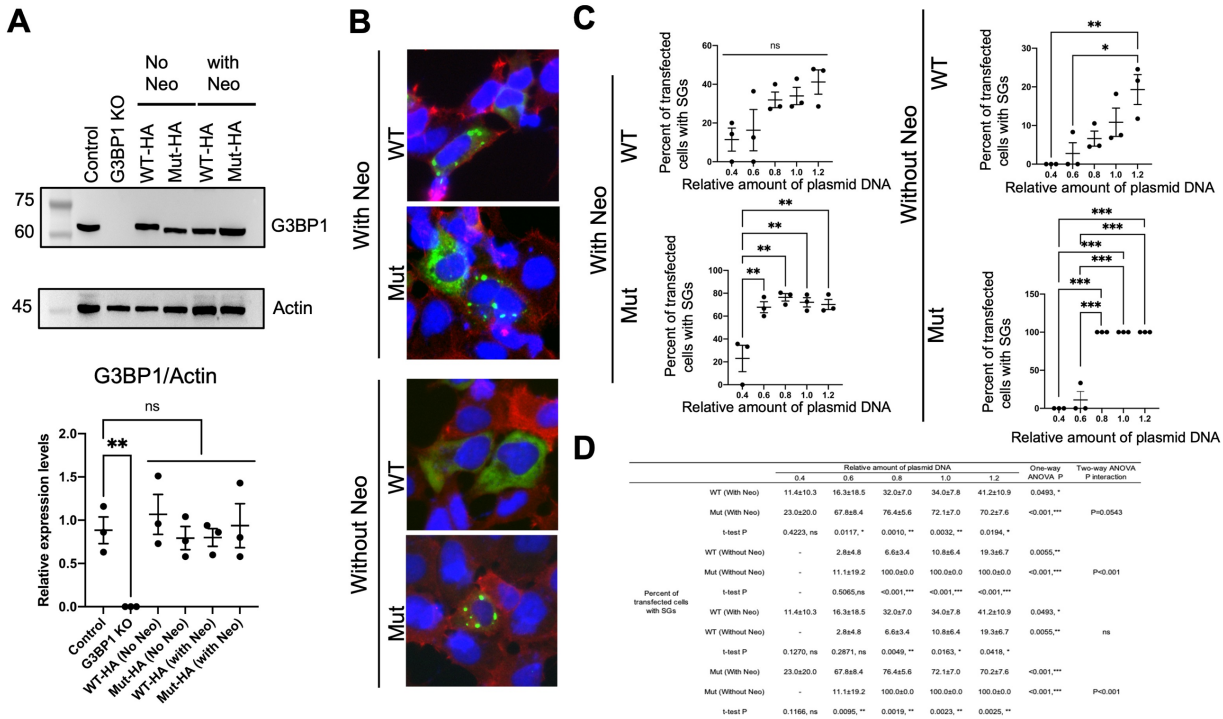

Fig. S6. Expression of Neo^R influences SG formation induced by exogenously expressed G3BP1.

(**A**) Western blotting against G3BP1. G3BP1 knock-out (KO) HEK293A cells expressing HA-tagged WT and mutant G3BP1 with or without Neo^R. Qantitation of relative intensity of band (bottom). Error bars represent S.D. from three independent counts. (**B**) Merged images of G3BP1 KO HEK293A cells expressing WT or mutant G3BP1-HA. HA-tag, FLNA, and nucleus were stained in green, red, and blue. 100 × 100 μm. (**C**) Quantitation of cells exogenously expressing G3BP1 by transfection of different relative amount plasmid DNA (0.4, 0.6, 0.8, 1.0, 1.2 times). P values are presented by * ($P \leq 0.05$), ** ($P < 0.01$) or *** ($P \leq 0.001$) on the graph, and ns (not significant). Error bars represent S.D. from three independent counts. (**D**) Statistical analyses. Ten cells were counted for 0.4 (relative amount of plasmid DNA) and over 50 cells were counted for 0.6~1.2 (relative amount of plasmid DNA), from three independent replicates. The results shown represent the mean (± S.D.) for three independent experiments.

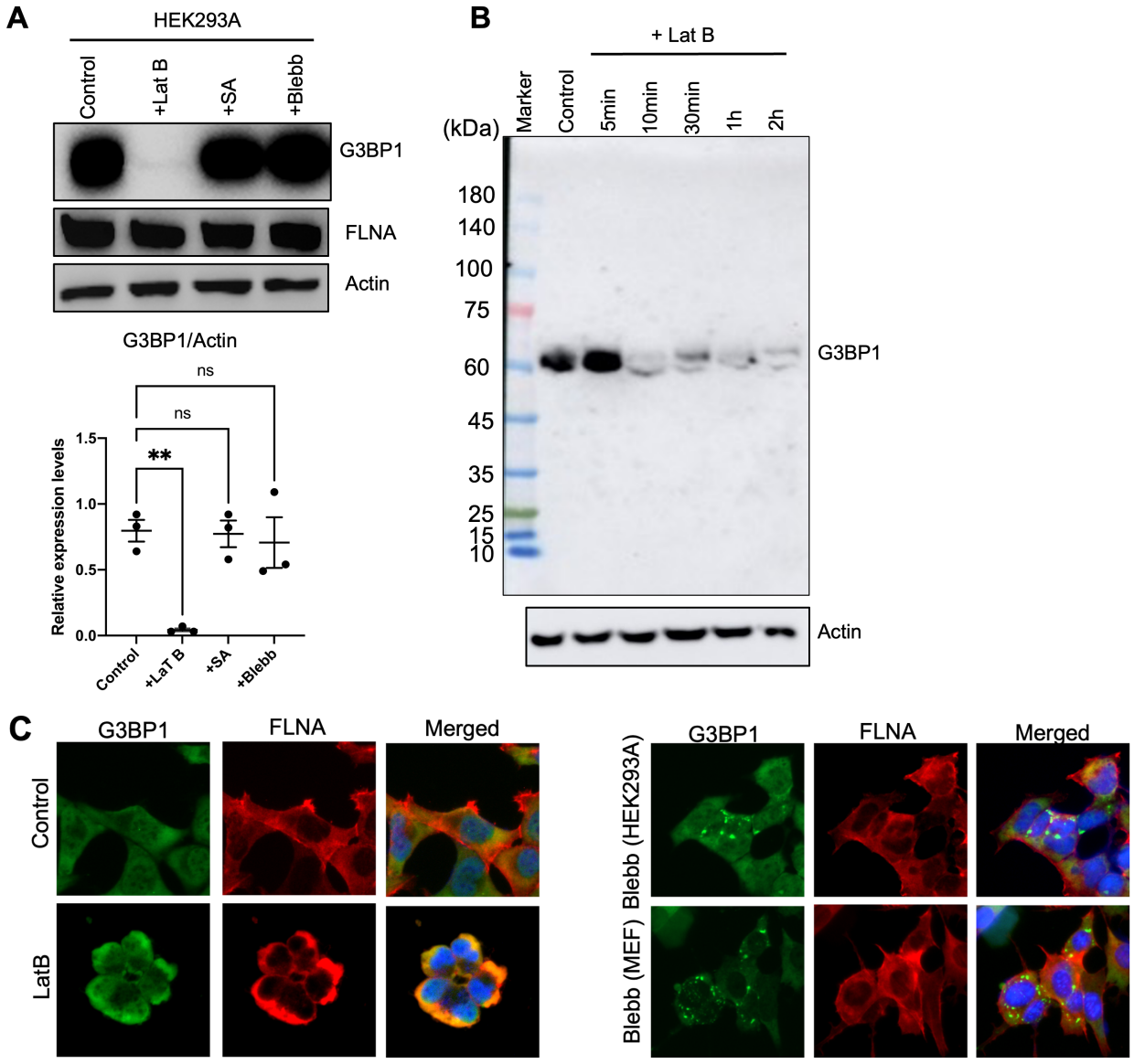

Fig. S7. Effects of latrunculin B, sodium arsenite, and blebbistatin on expression of G3BP1 and SG formation.

(**A**) Western blotting of cells treated with 5μM Latrunculin B (Lat B) for 2 hrs, 1.5 mM sodium arsenite (SA) for 1 hr, and 5μM blebbistatin (Blebb) for 2 hrs. The membrane was blotted with anti-G3BP1, anti-FLNA, and anti-actin. Relative intensities of the bands were quantitated on bottom panels. (n=3) (**B**) HEK293A cells were treated with 5μM Latrunculin B (Lat B) for various time as indicated and lysed with SDS sample buffer. Expression of G3BP1 and actin were detected by western blotting. (**C**) Immunofluorescent images of HEK293A cells treated with or without 5μM Latrunculin B (Lat B) or 5μM blebbistatin for 2 hrs. G3BP1, FLNA, and nucleus were stained in green, red, and blue. 100 × 100 μm.

Table S1. Potential FLNA-binding proteins identified by SILAC-based quantitative proteomics.

Click here to download Table S1

Table S2. Antibodies used in this study

Antibodies	Source	Identifier	Dilution
Anti-Histone H3 Monoclonal Antibody	Invitrogen	865R2	1:1000 (WB)
Anti-GFP Mouse Monoclonal Antibody	Thermo Fisher	MA5-15256	1:1000 (WB)
Anti-6x-His Tag Mouse Monoclonal Antibody	Thermo Fisher	MA1-21315	1:2000 (WB)
Anti-GFP Rabbit Polyclonal Antibodies	Abclonal (Wuhan, China)	AE011	1:2000 (WB)
Anti-G3BP1 Mouse monoclonal antibody	Proteintech (China)	66486-1-Ig	1:1000 (WB) 1:200 (IF)
Anti-HA Mouse monoclonal antibody	Proteintech (China)	66006-1-Ig	1:2000 (WB) 1:500 (IF)
Anti-FLNA antibody	anti-FLNA was outsourced (Pacific immunology, CA) using human FLNA repeat 1 and affinity purified using the antigen immobilized on NHS-Sepharose (GE Healthcare) as an affinity ligand		1:400 (IF)
Goat anti-mouse IgG (H+L)-horseradish peroxidase (HRP)	BioRad	172-1011	1:3000 (WB)
Goat anti-rabbit IgG (H+L)-HRP	BioRad	172-1019	1:3000 (WB)
Anti-Mouse IgG-Alexa Fluor Plus 488	invitrogen	A32723	1:400 (IF)
Anti-Mouse IgG-Alexa Fluor Plus 594	invitrogen	A32744	1:400 (IF)
Anti-Rabbit IgG-Alexa Fluor Plus 488	invitrogen	A32731	1:400 (IF)
Anti-Rabbit IgG-Alexa Fluor Plus 594	invitrogen	A32754	1:400 (IF)

Table S3. Oligonucleotide sequences used for PLA assay.

Name	Sequence
Probe-1	5′ azide – AAAAAAAAAATATGACAGAACTAGACACTCTT
Probe-2	5′ azide – AAAAAAAAAAGACGCTAATAGTTAAGACGCTT - 3 × 2′ O-methyl RNA uracil (UUU)
Circularization oligonucleotide 1	5′ phosphate – GTTCTGTCATATTTAAGCGTCTTAA
Circularization oligonucleotide 2	5′ phosphate – CTATTAGCGTCCAGTGAATGCGAGTCCGTCTAAGAGA GTAGTACAGCAGCCGTCAAGAGTGTCTA
Detection oligonucleotide	Cy3-CAGTGAATGCGAGTCCGTCT – 3 × 2′ O-methyl RNA uracil (UUU)